Final year project report

Computational simulations of stochastic processes: Investigating the shot noise model of free-electron laser SASE radiation and the Ornstein-Uhlenbeck theory of Brownian motion

Aaron Lalor-Fitzpatrick

Student No.: 15329051
Class: AP4
Supervisor: Dr. Lampros A. A. Nikolopoulos

2nd May 2019

Abstract

This project explores the behaviour of stochastic processes with the use of computational simulations. The stochastic analyses conducted in this project were that of a general Brownian process, in which Ornstein-Uhlenbeck theory was applied to the motion of a particle in a fluid following Maxwell-Boltzmann dynamics, and the application of shot noise theory to model the pulsed radiation resulting from self-amplification of spontaneous emission (SASE) in a free-electron laser (FEL). An investigation of random walks, arithmetic and geometric Brownian motion was also conducted to further model Brownian motion as a general stochastic process.

It was found that the simulations conducted describing Brownian motion as a stochastic process agree with the theoretical analysis. The statistical behaviour of SASE radiation resulting from electron shot noise was found to agree with the analysis done by Krinsky and Li (2006), in which analytical expressions derived for the unseeded SASE radiation is assumed to result from shot noise in the laser, where the arrival statistics of the pulse are characterised by the statistics of the electron bunch density in the undulator, which are approximated as being uniformly random in time for long pulses and follow a Gaussian distribution in time for short pulses.

Acknowledgements

I would like to thank my project supervisor, Dr. Lampros A. A. Nikolopoulos, for his excellent guidance throughout the duration of this project. He always encouraged learning of new concepts - producing high quality notes on more than one occasion - and provided a clear direction for this project, while still giving a healthy amount of space to excel in my work.

I would also like to thank Prof. John T. Costello for sharing his high level of expertise on the topics of free-electron laser physics and Fourier analysis, both of which feature heavily in this project.

Finally, I would like to thank Prof. Enda McGlynn for his superbly informative lesson and notes detailing how to write this project report, and for his continued support in the professional development element of this project.

Declaration

Name: Aaron Lalor-Fitzpatrick

Student ID Number: 15329051

Programme: AP4

Module Code: PS451

Assignment Title: Final Year Project Report

Submission Date: 15 April 2019

I understand that the University regards breaches of academic integrity and plagiarism as grave and serious.

I have read and understood the DCU Academic Integrity and Plagiarism Policy. I accept the penalties that may be imposed should I engage in practice or practices that breach this policy.

I have identified and included the source of all facts, ideas, opinions, viewpoints of others in the assignment references. Direct quotations, paraphrasing, discussion of ideas from books, journal articles, internet sources, module text, or any other source whatsoever are acknowledged and the sources cited are identified in the assignment references.

I declare that this material, which I now submit for assessment, is entirely my own work and has not been taken from the work of others save and to the extent that such work has been cited and acknowledged within the text of my work.

I have used the DCU library referencing guidelines (available at: `http://www.library.dcu.ie/LibraryGuides/Citing&ReferencingGuide/player.html`) and/or the appropriate referencing system recommended in the assignment guidelines and/or programme documentation.

By signing this form or by submitting this material online I confirm that this assignment, or any part of it, has not been previously submitted by me or any other person for assessment on this or any other course of study.

By signing this form or by submitting material for assessment online I confirm that I have read and understood DCU Academic Integrity and Plagiarism Policy (available at: `http://www.dcu.ie/registry/examinations/index.shtml`).

Name:_ _

Date:_ _

List of Figures

Contents

1 Introduction

1.1 Preamble

In the physical sciences, the exact analytical solution to a problem is what is typically most desired. However, this is not always possible. In fact, many physical systems exist which are too complex to model deterministically, and may only be modelled as a dynamic collection of random variables. This is known as a stochastic process.

The work presented in this paper fundamentally concerns itself with two stochastic processes: Brownian motion and shot noise. By taking advantage of pseudo random number generators readily accessible to modern computers, these stochastic processes can be simulated and applied to model physical applications. This project serves to do exactly that.

1.2 Project objectives

The key aims of this project, achieved by computational simulations, are listed below:

- To investigate random walks in 1, 2 and 3 dimensions as a model of Brownian motion
- To model the stochastic processes of arithmetic and geometric Brownian motion and compare simulated results to the analytical expressions for these processes
- To investigate the analysis of the Ornstein-Uhlenbeck theory of Brownian motion
- To model the electric field and intensity of single-shot FEL SASE radiation pulses in the time domain and frequency domain
- To attain the average behaviour of many FEL pulses using a sufficiently large sample of independent Monte Carlo trials
- To simulate the autocorrelation functions for FEL pulses and draw a comparison to the theoretical results predicted by Krinsky and Li based on shot noise the analysis done by Rice

2 Theory

2.1 Brownian motion

The physical phenomenon known as Brownian motion, named after renowned botanist Robert Brown[1], is the random motion of macroscopic particles within a fluid resulting from collisions with many microscopic particles (atoms and molecules) in that fluid.

Since Brownian motion is isotropic, particles are equally likely to undergo motion in all directions. Because this movement is due to a large ensemble of atoms and molecules that constitute the fluid, it is not possible to predict the direction and magnitude of motion deterministically. As such, Brownian motion must be treated using statistical mechanics. It is considered a stochastic process, as, due to the inability to measure the motion of all microscopic particles in a fluid, the motion of the particle is effectively random.

The model of Brownian motion as a stochastic process has many properties that make it useful in different applications of physics, finance, biology and mathematics[2].

2.1.1 History of Brownian motion

In 1827, the Scottish botanist Robert Brown observed mysterious movement of the particles inside pollen grains of the Clarkia Pulchella plant suspended in water. Looking at these particles under a microscope, he observed they moved very quickly in short, seemingly random bursts. This movement was constant and happened in all directions. Brown, curious to determine the reason for this movement, repeated this experimental observation with inorganic matter. What he found was that the inorganic matter exhibited the same movement, meaning its cause was not due to the presence of life, but could be found for any particles suspended in a fluid. Unfortunately Brown could not explain the reason for this phenomenon, and it would be many years later before Einstein and Smoluchowski provided a rigorous physical explanation.

The first mathematical description of Brownian motion was given by Thorvald N. Thiele in his paper on the least squared method in 1880.[3] Independently, in 1900, Louis Bachelier mathematically modelled Brownian motion as a stochastic process from random walks in his PhD thesis concerning the analysis of stock and options markets.[4] These were both works chiefly of a mathematical nature, not at all focused on the physical implications behind Brownian motion.

Albert Einstein and Marian Smoluchowski both produced similar, comprehensive paper on the subject of Brownian movement - both realising that the observed motion of a particle was due to collisions with atoms and molecules in the fluid surrounding it. The surrounding microscopic particles jiggle rapidly as a result of their thermal energy, and this energy gets imparted to the macroscopic particle in the form of kinetic energy upon collision. At any given time interval, the number of collisions that occur along different points on the surface of the particle is statistically near certain to be nonuniform, meaning the particle will experience a net acceleration in the direction towards the area with the relative lowest number of collisions per second. Both Einstein and Smoluchowski independently proposed the solution to explain Brownian motion as a means to describe the diffusion of particles in a fluid.[5][6] In doing so they both showed that the diffusion coefficient was related to the mean squared displacement of a particle exhibiting Brownian motion. They found that the mean squared displacement was proportional to the time interval of observation, and that the diffusion coefficient was the factor of proportionality.[1]

By relating known physical quantities to this solution, it was now possible to isolate the diffusion coefficient to be the only unknown variable and arrive at a solution to find Avogadro's number. This

[1] Einstein and Smoluchowski did however arrive at slightly different solutions, with Smoluchowski's result for the diffusion coefficient being a factor of 64/27 greater than that found by Einstein.

was a significant result as it allowed for Avogadro's number to be determined experimentally. This was subsequently done in 1908 by Jean Baptitse Perrin. In this verification he thus proved that matter was composed of atoms, and furthermore, determined experimentally the value of Avogadro's number. For these achievements Perrin was awarded the Nobel prize in Physics in 1926.[7]

2.1.2 Principles of Brownian motion

To understand the physics of Brownian motion it is important to be cognisant of the underlying mathematics that describe it. Brownian motion is an extension of the random walk model; where the number of steps is taken to be very large and the time interval is taken to approach zero, making it an effectively continuous process.[2]

Discrete Random walk The idea of a one-dimensional discrete random walk is considered as follows: A particle starts at a position x_0 at $t = 0$. After each discrete passing unit of time, the particle will undergo a "jump" s_i. The magnitude of this jump remains constant for each step, but the direction can either be left or right relative to x_0**.** The direction of each jump is random and the probability of the particle moving a particular way is independent from other jumps. After n steps, the position of a point particle x_n at time t_n is a random quantity, given by

$$x_n = x_0 + \sum_{i=1}^{n} s_i, \ i = 1, 2, ... \tag{2.1}$$

The probabilities of the particle moving right (p) and left $(1-p)$ are given as follows:

$$P(s_i) = \begin{cases} p, & s_i = \Delta x \\ 1-p, & s_i = -\Delta x \end{cases} \quad i = 1, 2, ... \tag{2.2}$$

where p is the drift parameter of the particle ($p = \frac{1}{2}$ corresponds to zero net drift to the left or right).

After n steps, the end position is given by $x_n = k\Delta x = n_+\Delta x - n_-\Delta x$, where Δx is the fixed step size. Note that $n_+ + n_- = n$ and $k = n_+ - n_-$. The probability of n_+ jumps to the right occurring, out of a total of n jumps is given by the following binomial distribution:

$$P(x_n = k\Delta x) = \binom{n}{n_+} p^{n_+}(1-p)^{n_-} \tag{2.3}$$

However, since $n_\pm$ can be written in terms of n, k as $n_+ = \frac{n+k}{2}$, $n_- = \frac{n-k}{2}$, the probability that $x_n = k\Delta x$ can be written as:

$$P(x_n = k\Delta x) = \binom{n}{\frac{n+k}{2}} p^{\frac{n+k}{2}}(1-p)^{\frac{n-k}{2}}, \ k = -n, -n+2, ..., n-2, n \tag{2.4}$$

Note that k can not take all values from $-n$ to n, there is a step size of 2. This result can be visualised using the case of $n = 2$. The final position of the particle can either be $-2, 0$, or 2. If n is an odd number, all possible values for k will be odd. The opposite is true if n is even.

In the case of one-dimensional Brownian motion, let's assume that $p = 1 - p = 0.5$, i.e. the chance of a jump to the left occurring is just as likely as a jump to the right. The probability distribution is thus given as

[2] The mathematical description of the random walk process and its relation to Brownian motion has been sourced heavily from the project supplement notes material: Nikolopoulos, L.A.A. Notes on Brownian Movement modelling. 2018:5-10.

$$P(x_n = k\Delta x) = \binom{n}{\frac{n+k}{2}} \frac{1}{2}^n,\ k = -n, -n+2, ..., n-2, n \tag{2.5}$$

For simplicity, let initial position $x_0 = 0$. It can be shown that the expectation value of this distribution $E[x_n] = x_0 = 0$ and the variance $V[x_n] = n\Delta x^2$.

If the number of steps is taken to be large, the random walk can exhibit an interesting property as a result of the Central Limit Theorem (CLT). According to CLT, if a distribution is composed of a large number of independent arbitrary distributions, it will tend towards a Gaussian (normal) distribution with the same mean and standard deviation. Thus the distribution will be equivalent to the Gaussian, $N(x; \mu = 0, \sigma^2 = n\Delta x^2)$.

This can be written as

$$\lim_{n>>1} P(x_n = k\Delta x) \to P(x < \tilde{x} < x + \Delta x) = N(x; 0, n\Delta x^2) \tag{2.6}$$

Where $\tilde{x}$ denotes the continuous random variable instead of the discrete random variable x_n.

Interestingly, in theory, the mean distance squared from the initial position following n jumps is proportional to $\sim n$.

Continuous time limit random walk True Brownian motion is effectively continuous. As such, the time step duration used when modelling a continuous random walk will be taken to approach 0, and the number of steps must approach infinity.

Starting at time $t_0 = 0$, after n jumps, $\Delta t = t - t_0$ is:

$$\Delta t = n(t_{i+1} - t_i) = n\tau \ \longrightarrow\ n = \frac{\Delta t}{\tau} \tag{2.7}$$

By reversing the standard discretization procedure of a continuous variable (in this case time), we require the number of steps to approach infinity ($n \to \infty$), with a time step τ decreasing accordingly ($\tau \to 0$).

The rate of growth for n and decrease of τ should be such that $\Delta t < \infty$.

The continuous probability will then be:

$$\lim_{n\to\infty, \tau\to 0} P(x_n = k\Delta x) \to P(x < \tilde{x} < x + \Delta x) = N(x; 0, \frac{\Delta x^2}{\tau}\Delta t) \tag{2.8}$$

Since $\tau \to 0$, the value of Δx (the size of each step) should decrease accordingly in a way such that the limit of $\frac{\Delta x^2}{\tau}$ is finite.

Eventually we arrive at the following limit:

$$\lim_{n\to\infty, \tau\to 0} \frac{\Delta x^2}{\tau} \to \sigma^2 \tag{2.9}$$

And hence:

$$P(x < \tilde{x} < x + \Delta x) = N(x; 0, \sigma^2 \Delta t) \tag{2.10}$$

For infinitesimal change in position dx in time interval dt, we have that $dx(t)$ is normally distributed as,

$$dx(t) = N(x; 0, \sigma^2 dt) \tag{2.11}$$

Wiener process The time-dependent random quantity distributed normally with $\mu = 0, \sigma = t$, denoted as $B(x;t)$ (or $W(x;t)$), is called the Wiener process[8], and is fully defined by the following basic properties:

1. $B(x;0) = 0$
2. Independent increments: Increments of $dB(x;t_i) = B(x;t_i + \Delta t) - B(x;t_i)$ are independent of each other $(i = 1, 2, ...)$.
3. Gaussian property: Increments are normally distributed: $dB(x;t) = B(x;t') - B(x;t) \sim N(x;0,dt)$,where $dt = t' - t > 0$. Thus the mean and variance for this process are given by:

$$\begin{aligned} \mathbb{E}[dB(x;t)] &= 0 \\ \mathbb{V}[dB(x;t)] &= dt \end{aligned} \tag{2.12}$$

4. The Wiener process is a function that is everywhere continuous but nowhere differentiable.

Next, using the linear transformation property of a normal distribution, i.e., for a given normal random variable $\tilde{y} = N(y;\mu,\sigma^2)$, if $\tilde{w} = a\tilde{y} + b$, then $\tilde{w} = N(w;a\mu + b, a^2\sigma^2)$, we have, for a Brownian process,

$$dx(t) = N(x;0,\sigma^2 dt) = \sigma\sqrt{dt}\tilde{N} = \sigma dB(x;t) \tag{2.13}$$

where $\tilde{N} \equiv N(x;0,1)$.

In general, for a Brownian process with nonzero drift ($\mu \neq 0$), the process is described by $dx(t) = N(x;\mu dt, \sigma^2 dt)$, and hence, by the same transformation property as above,

$$dx(t) = \mu dt + \sigma\sqrt{dt}\tilde{N} = \mu dt + \sigma dB(t) \tag{2.14}$$

To arrive at the most general formulation of a Brownian process, one must assume that in general, the parameters μ and σ are not constant, but rather, depend on time t and the process itself, $x(t)$, i.e.,

$$\begin{aligned} \mu &= \mu(x(t),t) \\ \sigma &= \sigma(x(t),t) \end{aligned} \tag{2.15}$$

This generalisation is known as an Itô stochastic process. Applying this generalisation to a random quantity $x(t)$ described by Brownian motion gives the process in its most general form:

$$dx(t) = \mu(x(t),t)dt + \sigma(x(t),t)dB(t) \tag{2.16}$$

2.1.3 Arithmetic Brownian motion

By applying the generalised formulation of Brownian motion from Eq. (2.16) for a process specified by constant μ and σ, one specifies the process known as arithmetic Brownian motion given by,

$$dx(t) = \mu dt + \sigma dB(t) \tag{2.17}$$

By integrating the expression above, one arrives at the following exact solution,

$$x(t) = x(0) + \mu t + \sigma B(t) \tag{2.18}$$

since $B(0) = 0$.

This process has the following mean and variance values:

$$\begin{aligned} \mathbb{E}[x(t)] &= x(0) + \mu t \\ \mathbb{V}[x(t)] &= \sigma^2 t \end{aligned} \tag{2.19}$$

Thus, arithmetic Brownian motion is said to model the time evolution of a random quantity x to depend on:

- One fully deterministic part (drift), μ, which here coincides with the mean value for the process
- A random part, with values randomly distributed around 0, according to the normal distribution and with the standard deviation specified by $\sigma\sqrt{dt}$.

From above it's clearly seen that for a process described by arithmetic Brownian motion, both the mean and variance grow linearly with time. It should also be noted that since there is nothing preventing $x(t)$ to take on negative values, it means that in practice arithmetic Brownian motion is an unsuitable model for random quantities that take only positive values, such as for example stock prices.

2.1.4 Geometric Brownian motion

A geometric Brownian process is one in which the Wiener process describes the stochastic behaviour of the relative change of a random quantity, as opposed to arithmetic Brownian motion, where it described the behaviour of the quantity itself. This is expressed mathematically as,

$$\frac{dx(t)}{x(t)} = \mu dt + \sigma dB(t) \ \sim N(\mu dt, \sigma^2 dt) \tag{2.20}$$

It can be found that the analytical solution for a geometric Brownian process is given by,

$$x(t) = x(t')e^{[(\mu - \frac{\sigma^2}{2})(t-t') + \sigma(B(t) - B(t'))]} \tag{2.21}$$

at the elapsed time $t - t$', provided that x is known at some time t' earlier. Using the above, one can see that when t' $= 0$ we have $B(0) = 0$ and thus the equation simplifies to,

$$x(t) = x_0 e^{[(\mu - \frac{\sigma^2}{2})t + \sigma B(t)]} \tag{2.22}$$

where $x_0 = x(0)$ is the initial value of the random quantity.

By taking the natural log of this equation one arrives at,

$$ln(x(t)) = ln(x_0) + (\mu - \frac{\sigma^2}{2})t + \sigma\sqrt{t}\tilde{N} \tag{2.23}$$

By applying the same transformation property of a normal distribution as above it can be seen that,

$$G(t) = ln(x(t)) = N(lnx_0 + (\mu - \frac{\sigma^2}{2})t, \sigma^2 t) \tag{2.24}$$

Which infers that $x(t)$ is lognormally distributed[3] rather than normally distributed. It is now straightforward to see that the expectation value and mean for this process are given by,

$$\begin{aligned} \mathbb{E}[G(t)] &= lnx_0 + (\mu - \tfrac{\sigma^2}{2})t \\ \mathbb{V}[G(t)] &= \sigma^2 t \end{aligned} \tag{2.25}$$

2.1.5 Ornstein-Uhlenbeck Brownian motion

Ornstein-Uhlenbeck Brownian motion[9] is described by having a drift rate proportional to the current position of the random variable and a constant standard deviation, as shown,

$$\mu(X(t), t) = -\mu_0 X(t), \qquad \sigma = cnst. \tag{2.26}$$

Two examples of processes described by Ornstein-Uhlenbeck Brownian motion are the irregular motion of a particle on the surface of a liquid, and the thermal electrical current in conductors (known as Johnson–Nyquist noise, or "white noise"[10, 11]). In this paper, analysis is focused on the particle motion on the surface of a fluid.

Fluctuations in speed of a particle in a fluid A particle, m, is considered, moving in one-dimension subject to numerous collision with fast moving molecules (with respective masses much smaller than m). According to Newtonian mechanics, the particle's motion can be determined by solving a system of equation of motion for all involved particles, simultaneously. Due to the very large number of particles present in a measurable physical system (on the order of Avogadro's number), an exact analytical solution can not be found for such a system. As such, one assumes that the statistical properties of the molecular gas are not influenced by the massive particle's motion and as such their state at temperature T should always be at a thermodynamic equilibrium with speeds following the Boltzmann-Maxwell distribution. This dynamic balance implies that the exchange of energy between the particle, m, and the rest of the molecular gas, is equal at all times, meaning the statistical properties are time invariant. Thus one may conjecture that the average value of the kinetic energy must be:

$$\left\langle \frac{1}{2} k_B T \right\rangle_{eq} = \left\langle \frac{1}{2} m v^2 \right\rangle_{eq}. \tag{2.27}$$

At the same time the particle's Newtonian dynamics is modelled by:

$$m\dot{v}(t) = -\gamma v(t) + F(t), \tag{2.28}$$

where $-\gamma v(t)$ is the viscosity drag force tending to decelerate the particle and a random force, $f(t)$, whose statistical properties depend on the surrounding environment.

Defining $1/\tau = \gamma/m$ and $f(t) = F(t)/m$, Eq. (2.28) can be rewritten as,

$$\dot{v}(t) = -\frac{1}{\tau} v(t) + f(t). \tag{2.29}$$

To proceed further one needs to assume the statistical properties of $f(t)$ since no analytical expression is possible for random processes by definition. As such one assumes typical values where the Brownian particle is spherical of radius $R \sim 0.5\ \mu m$ and mass $m \sim 8 \times 10^{-9}$ kg. For liquid one assumes viscosity $\eta \sim 0.01$ and by making use of Stoke's law[12] where $\gamma \sim 6\pi\eta R$ one arrives at a value for the decay time,

$$\tau \sim 10^{-7}\ sec \tag{2.30}$$

[3] The lognormal distribution is given by $L(y; \mu, \sigma) = \frac{1}{y\sigma\sqrt{2\pi}} e^{-\frac{(lny-\mu)^2}{2\sigma^2}}$

By assuming that the collisions occur roughly with a rate of about $10^{12} - 10^{13}$ collisions per second, this means that there are $\sim 10^6$ collisions with other particles before effects of the deterministic part shows up. Thus it is reasonable to assume that the correlation time between values of the random force $f(t)$ and $f(t')$ must be of the order of 10^{-12}, much shorter than τ. It is then a valid approximation to take the following statistical properties for the random collisional force $f(t)$:

$$\langle f(t) \rangle = 0, \qquad \langle f(t) f(t') \rangle = D\delta(t_1 - t_2), \tag{2.31}$$

where $\delta(t_1 - t_2)$ is the Dirac-delta function. D in above expression is known as the *diffusion* constant. Eq. (2.28) may be rewritten to fit the general Brownian equation if expressed as,

$$f(t) = \sqrt{D} N(0, 1/dt) = \frac{\sqrt{D}}{\sqrt{dt}} N(0, 1) \tag{2.32}$$

Then, Eq. (2.28) takes the following form,

$$dv(t) = -\frac{1}{\tau} v(t) dt + \sqrt{D}\sqrt{dt} N(0, 1), \tag{2.33}$$

known as the Ornstein-Uhlenbeck (OU) stochastic process. What remains to determined is the standard deviation of the process, given by $\sigma = \sqrt{D}$. For this the equilibrium relation Eq. (2.27) is used. So, it is necessary to evaluate the average value of v^2 for the OU process, as follows. Integration of Eq. (2.28) gives the formal solution,

$$v(t) = v_0 e^{-t/\tau} + \int_0^t dt' e^{-(t-t')/\tau} f(t). \tag{2.34}$$

Taking the square of this expression one arrives at,

$$v^2(t) = v_0^2 e^{-2t/\tau} + 2v_0 e^{-t/\tau} \int_0^t dt' e^{-(t-t')/\tau} f(t) + \int_0^t dt' \int_0^{t''} dt'' e^{-(t-t')/\tau} e^{-(t-t'')/\tau} f(t) f(t')$$

By taking the ensemble average $\langle v^2(t) \rangle$ after using Eq. (2.31) it is found,

$$\begin{aligned} \langle v^2(t) \rangle &= \langle v_0 e^{-2t/\tau} \rangle + \int_0^t dt' \int_0^{t''} dt'' e^{-(t-t')/\tau} e^{-(t-t'')/\tau} D\delta(t' - t'') \\ &= v_0 e^{-2t/\tau} + D \int_0^t dt' e^{-(t-t')/\tau} e^{-(t-t')/\tau} \\ &= v_0 e^{-2t/\tau} + D \int_0^t dt' e^{-2(t-t')/\tau} = v_0 e^{-2t/\tau} + \frac{D\tau}{2}(1 - e^{-2t/\tau}) \end{aligned} \tag{2.35}$$

where the δ-function (definition) property $\int_a^b dx' f(x')\delta(x - x') = f(x)$ was used. From the latter equation one sees that at the thermodynamic equilibrium, reached in steady-state ($t \to \infty$),

$$\langle v^2 \rangle_{eq} = \frac{D\tau}{2}. \tag{2.36}$$

From this equation and Eq. (2.27) it is found that,

$$D = \frac{2k_B T}{m\tau} = \frac{2k_B T/m}{\tau}. \tag{2.37}$$

Thus, in the context of the OU equation one finally obtains:

$$dv(t) = -\frac{1}{\tau} v(t) dt + \frac{\sigma_0}{\sqrt{\tau}} \sqrt{dt} N(0, 1), \tag{2.38}$$

$$\tag{2.39}$$

$$\mu = -\frac{1}{\tau} v(t), \qquad \sigma = \frac{\sigma_0}{\sqrt{\tau}} \tag{2.40}$$

$$\frac{1}{\tau} = \frac{\gamma}{m} = \frac{6\pi\eta R}{\mu}, \qquad \sigma_0 = \sqrt{2\langle v^2 \rangle_{eq}} = \sqrt{2k_B T/m} \tag{2.41}$$

2.2 Characterisation of a stochastic process

2.2.1 Autocorrelation

Autocorrelation is defined as the correlation of a signal with a delay of itself. It is a function of the time delay between the signal and its copy. Autocorrelation is a useful tool in studying the behaviour of stochastic processes in the time domain and frequency domain. The autocorrelation of a signal $X(t)$ is defined by,

$$R_x(t_1, t_2) = \langle X(t_1)X^*(t_2)\rangle \tag{2.42}$$

The autocorrelation function has the following three properties:

1. $R_X(0) = \left\langle X^2(t)\right\rangle \equiv \mathbb{E}[X(t)^2]$ (mean square value of the process at $\tau = 0$)
2. $R_X(\tau) = R_X(-\tau)$ (autocorrelation function is even)
3. $|R_X(\tau) \leq R_X(0)\ \forall\ \tau$ (Maximum value of autocorrelation function is at $\tau = 0$)[4]

As a result of the third property above, one can get what's known as the expected (or average) power of the process, $\mathbb{E}[X(t)^2]$, by getting the autocorrelation at $\tau = 0$

2.2.2 Ergodicity

A stochastic process is said to be ergodic if its statistical properties can be deduced from a single. sufficiently large, random sample of the process. The reasoning for this is that any collection of random samples of a process must represent the average statistical properties of the entire process. Conversely, a process that is not ergodic is a process that changes its behaviour at an inconsistent rate. This paper only deals with ergodic processes.

2.2.3 Wide-sense stationary processes

Random processes may be classified based on many different criteria. Of paramount importance is whether or not a random process can be considered stationary. A random process is strict-sense stationary if all of its statistical properties are unchanging with time. This characterisation isn't widely applicable; many real-life processes are not strictly stationary. Another common form of stationarity is that of wide-sense stationarity, which is significantly more commonly observed than strict-sense stationarity. A random process $X(t)$ is said to be wide-sense stationary (WSS) if its autocorrelation function and mean are time invariant, and if the second moment of the process is finite. More precisely,

- $\mathbb{E}[X(t)] = \mu$, independent of t
- $R_x(t_1, t_2)$ is a function only of the time difference $t_2 - t_1$, i.e. $R_x(t, \tau) = R_x(\tau)$
- $\mathbb{E}[X(t)^2] = R_x(\tau = 0) < \infty$

[4] This property is a consquence of what's known as the Schwartz inequality.

2.2.4 Power spectral density

For a wide-sense stationary process that is continuous over all time, one can attain what's known as the power spectral density (PSD); this describes how the power content of a signal is distributed with respect to frequency. Power spectral density is typically used in characterisation of broadband random signals, such as shot noise.

For a wide-sense stationary process, the power spectral density is defined as the Fourier transform[5] of the autocorrelation function of a signal, expressed as,[6]

$$S_I(\omega) = \int_{-\infty}^{\infty} R_I(\tau) e^{-i\omega\tau} d\tau \tag{2.43}$$

2.2.5 Characterisation of shot noise

Shot noise is a type of noise originating from the discrete nature of electric charge[7]. Shot noise in electronic circuits consists of random fluctuations in current. This is because current is not continuous, rather, it consists of a flow of discrete charges (electrons). The instantaneous current density due to random electron emission can then be expressed by $j_e = -\sum_j \delta(t - t_j)$, where t_j is the random time of spontaneous electron emission.

This type of noise was investigated by Schottky in 1918 in his publication on spontaneous current fluctuations in electric conductors[15]. With very small currents, particularly when taking measurements on short time scales (and by Fourier analysis, this means taking measurements with broader bandwidths), shot noise can be significant. It was found by Schottky that in the case of shot noise resulting from current produced by electrons, the one-sided power spectral density is given by,

$$S_I(\omega) = 2q_e I_{DC} \tag{2.44}$$

where q_e is the electron charge and I_{DC} is the average current. As can be seen from Eq. (2.44), the power spectral density does not depend on the frequency. This is because shot noise is white (equal power across all frequencies).

Shot noise has a Poisson distribution. This is because the noise is a result of a discrete number of event occurrences (emission of electrons or photons), which occur randomly and independently, and the probability of an event occurring in a given time interval does not vary over time. As such, for a process described by shot noise, a sufficiently long sample of events will produce a valid approximation for the overall statistical properties of the process. Hence, shot noise is an ergodic process.

An important consequence of the ergodicity of shot noise is that the time autocorrelation of a sufficiently long sample will equal the complete statistical autocorrelation function. The autocorrelation function of a shot noise process is time invariant. From this it is clear to see that shot noise is a wide-sense stationary random process.

In 1944-45, Rice[16] gave an extensive analysis of shot noise when the underlying Poisson process has a constant intensity. Using the analysis done by Rice, other physical systems which exhibit shot noise-like phenomena can be modelled accurately, such as the stochastic behaviour of free-electron laser radiation, in which shot noise inside the laser leads to a process called self-amplification of spontaneous emission.

[5] The Fourier transform of a function of time, $f(t)$, is the decomposition of $f(t)$ into its constituent frequencies. In general this is given by $\mathscr{F}\{f(t)\} = F(\omega) = \int_{-\infty}^{+\infty} f(t) e^{-i\omega t}$

[6] This is known as the Wiener-Khintchine theorem[13, 14]

[7] The term "shot noise" also applies to photon counting in optical devices, where the shot noise observed is associated with the particle nature of light.

2.3 Free-electron lasers

A free-electron laser (FEL) is a type of laser in which the lasing medium consists of high-speed free electrons travelling through a magnetic structure. FELs are very tuneable and currently have the widest frequency range of any laser type, ranging in wavelength from x-rays to microwaves. The electron beam in a free-electron laser has very low emittance, meaning the the radiation produced will be small, and thus have high brightness. FEL radiation has many applications in atomic physics, such as studying the structure and dynamics of atomic and molecular systems using photoionization techniques.[17, 18]

To start the FEL, a beam of electrons is first created. This is done using a drive laser, which generates a precise UV pulse, which travels to the FEL's injector gun and strikes the surface of a copper plate inside the gun. This copper cathode emits a burst of electrons via the photoelectric effect, which are then guided into a linear accelerator. This process happens periodically with the pulses of UV light.

This beam of free electrons is then accelerated by radio frequency (RF) cavities in the linear accelerator to close to the speed of light. These now relativistic electrons then pass through an insertion device known as an undulator[8] – a series of periodic arrangements of magnets with alternating poles, that create a side-to-side magnetic field. By the Lorentz force, the moving electrons oscillate transversely. The acceleration of a charged particle leads to emission of electromagnetic radiation by Bremsstrahlung (braking radiation), and this is what occurs in an FEL due to the periodic acceleration of the relativistic electrons.[9]

Because of relativistic speed of the electrons, the emitted radiation is compressed into a narrow cone in the direction of motion instead of propagating isotropically. This is known as a relativistic beam, and is highly collimated. This electromagnetic radiation is monochromatic but still incoherent, owing to the fact that the electromagnetic waves from randomly distributed electrons interfere constructively and destructively in time.

Mirrors at each end of the undulator act to create an optical cavity, causing the synchrotron radiation to form a standing wave.[10] The radiation becomes sufficiently strong that the transverse electric field component of the beam interacts with the transverse electric current created by the oscillating electron motion, causing some electrons to gain energy and others to lose energy, depending on the direction of the optical electric field at the moment of interaction. This acceleration or deceleration of electrons upon interaction with this inhomogeneous oscillating electric field is known as the ponderomotive force. Effectively, the slower-moving electrons will "catch up" with the faster-moving electrons. This modulation in kinetic energy leads to modulations in the linear electron density along the beam. The electrons are thus longitudinally separated into "microbunches", separated by one optical wavelength. This effect is known as self-amplification of spontaneous emission (SASE).

Whereas the undulator alone would cause the electrons to radiate independently (and thus incoherently), the radiation emitted by the bunched electrons is in phase, and as a result the fields add together coherently. Due to this effect, the radiation intensity inside the FEL grows, causing further microbunching of the electrons, which continue to radiate in phase with each other. This process continues until the electrons are completely microbunched and the radiation reaches saturation power (several orders of magnitude higher than that of undulator-induced radiation).

In most cases the theory of classical electrodynamics adequately describes the behaviour in an FEL. However, for short-wavelength light, such as EUV[11] and x-ray radiation, quantum effects of electron recoil and shot noise must be considered. Although capable of producing a high degree of spatial coherence, the problem with radiation from SASE free-electron lasers is the lack of temporal coherence due to a noisy start-up process. To mitigate this, the FEL can be seeded with an external laser that is tuned

[8] Undulators are typically used in modern FELs, although another type of insertion device, known as a wiggler, can also be used.

[9] Electromagnetic radiation produced in this way is known as synchrotron radiation.

[10] Alternatively, an external excitation laser is used here instead.

[11] Extreme ultraviolet

to the resonance frequency of the FEL. This seed radiation can be produced using conventional means, such as using high-harmonic generation (HHG) using a pulsed optical laser. However, this technique is unfeasible for FELs operating in very short wavelengths such as x-rays, due to the lack of conventional x-ray lasers.[12]

2.3.1 Characteristics of emitted FEL radiation

It is known that radiation produced by free-electron lasers can be characterised by its high spatial coherence. However, because SASE begins from shot noise in the electron beam within the laser, the temporal coherence of an unseeded FEL pulse is poor. This incoherence arises because the total radiated field is composed of the radiation contributions of many individual electrons, each having its own frequency spectrum, $E_j(z,\omega), j = 1, 2, \ldots, N_e$ and arriving at random times, t_j. This random field can be represented mathematically as a pulse train over the individual pulses, generated by the current density from each electron's contribution, denoted $j_e = -\sum_{j=1}^{N_e} \delta(t - t_j)$. The statistical properties of the pulse train then depend on the statistics of the arrival times t_j. The arrival times t_j are directly related to the electron bunch density distribution within the microbunches, and thus so too does the temporal profile of the emitted radiation.

In the case of a long electron bunch characterised by a uniform density, the statistical properties of the SASE output are modelled by applying the analysis of the shot noise process developed by Rice.[13] For a bunch length (duration) of T_b, the density function describing the arrival time t_j is given by

$$p_t j(t) = \begin{cases} \frac{1}{T_b}, & -\frac{T_b}{2} < t < \frac{T_b}{2} \\ 0, & otherwise \end{cases} \tag{2.45}$$

For an electron bunch density described by a Gaussian distribution, work by Krinsky and Li (2006)[19] show that although there is no translational time invariance of the field, the statistical behaviour of the radiation can be determined in terms of a stationary Gaussian stochastic process.

In this case the electron bunch density profile is given by

$$w_b(t) = \frac{1}{\sigma_e \sqrt{2\pi}} e^{-\frac{t^2}{2\sigma_e^2}} \tag{2.46}$$

Near saturation, the radiated electric field produced from FEL SASE is given by

$$E(z,t) = A(z,t) e^{(ik_r z - i\omega_r t)} \tag{2.47}$$

where z is the location along the undulator at which SASE is observed and t is the temporal position in the radiation pulse.

In the case of an electron beam with a long, flat-top electron bunch profile, the SASE electric field before saturation is the superposition of a large number of electromagnetic wave packets. Within classical theory, along one dimension the slowly-varying envelope can be approximated by

$$A(z,t) = A_0(z) \sum_{j=1}^{N_e} e^{\left[i\omega_r t_j - \frac{(t - t_j - z/v_g)^2}{4\sigma^2}\right]} \tag{2.48}$$

[12] This limitation can be circumvented for x-ray FELs by self-seeding the laser with its own beam, but this technique is not explored in this paper.

[13] Although Rice's work was on the study of shot noise in electrical circuits, much of the analysis can be applied to characterise SASE output radiation, particularly that described by uniform electron bunch density.

where N_e is the total number electrons in the electron bunch, t_j is the arrival time of the j^{th} electron at the undulator entrance, and v_g is the group velocity of each wave packet. By letting $z = 0$, the position at the undulator entrance, this simplifies to

$$A(t) = A_0 \sum_{j=1}^{N_e} e^{\left[i\omega_r t_j - \frac{(t-t_j)^2}{4\sigma^2}\right]} \tag{2.49}$$

The intensity of a given pulse can be found from the electric field, by,

$$I(t) = |E(t)|^2 \tag{2.50}$$

For ultrashort FEL pulses, the assumption of uniform electron pulse density is no longer suitable. In this regime a better approximation of the bunch density is that of a Gaussian distribution along the electron bunch. In the case of a Gaussian electron bunch profile, the output radiation as a function of time becomes a non-stationary stochastic process. With the introduction of a smoothing factor $\chi = 1 + \frac{i}{\sqrt{3}}$, the field can be approximated by

$$A(t) = A_0 \sum_{j=1}^{N_e} e^{\left[i\omega_r t_j - \frac{(t-t_j)^2}{4\sigma^2}\chi\right]} \tag{2.51}$$

The output radiation of an FEL as a function of time exhibits spiking. The width of the intensity spikes can be characterised by the coherence time of the pulse, given by,

$$t_{coh} = \int d\tau |g_1(\tau)|^2 \tag{2.52}$$

.

where $g_1(\tau)$ is the time-averaged first-order normalised autocorrelation function (also known as the degree of coherence), given by,

$$g_1(\tau) = \frac{\left\langle \int dt E(t) E^*(t+\tau) \right\rangle}{\left\langle \int dt |E(t)|^2 \right\rangle} \tag{2.53}$$

for a wide-sense stationary process.

However, it should be noted that in general, the normalised first-order autocorrelation function is typically defined in terms of two times t_1 and t_2, as,

$$g_1(t_1, t_2) = \frac{\langle A(t_1) A^*(t_2) \rangle}{\sqrt{\langle |A(t_1)|^2 \rangle \langle |A(t_2)|^2 \rangle}} \tag{2.54}$$

and the second-order autocorrelation, as

$$g_2(t_1, t_2) = \frac{\left\langle |A(t_1)|^2 |A(t_2)|^2 \right\rangle}{\langle |A(t_1)|^2 \rangle \langle |A(t_2)|^2 \rangle} \tag{2.55}$$

The coherence time of a pulse is the time at which its electric field may be considered temporally coherent, meaning that on average, its phase is predictable. In general, a chaotic pulse will have a low coherence time. The number of longitudinal modes present in the output pulse depends on the coherence time. An ideal (coherent) pulse will have one central mode

For an FEL pulse produced by SASE with a constant electron bunch density, the first-order autocorrelation can be approximated by[20],

$$g_1(\tau) = e^{-\frac{\sigma_\omega^2 \tau^2}{2}} \tag{2.56}$$

In which case it follows that, for $t_{coh} << T_b$,

$$t_{coh} = \frac{\sqrt{\pi}}{\sigma_\omega} \tag{2.57}$$

The number of modes is given by

$$\frac{1}{M} = \frac{t_{coh}}{T_b} \tag{2.58}$$

Since for a Gaussian bunch density the output radiation is non-stationary, the time-averaged autocorrelation function from Eq. (2.53) to calculate the coherence time. In the case where the coherence time is small compared to the electron bunch distribution deviation ($\sigma << \sigma_b$), the coherence time and number of modes found for a pulse with Gaussian density can be approximated as:

$$t_{coh} \cong \frac{\sqrt{\pi}}{\sigma_\omega} \tag{2.59}$$

$$M \cong \frac{2\sigma_\tau \sqrt{\pi}}{t_{coh}} \tag{2.60}$$

3 Methods

3.1 Investigation of models described by Brownian motion

This section outlines the procedures carried out in this project to investigate the behaviour of several Brownian models, namely; random walks, arithmetic and geometric Brownian motion, and Ornstein-Uhlenbeck Brownian motion.

3.1.1 Random walk simulations

Variation of number of trials taken To investigate the effect of increasing the number of trials on the accuracy of the random walk simulations, Monte Carlo trials were conducted on one-dimensional random walks and frequency distributions of final particle positions were plotted and compared with the predicted binomial distribution.

Variation of drift parameter By varying the drift parameter p and conducting Monte Carlo random walks, the effect of drift on the particle's motion was investigated. This was done for predicted leftward drift and rightward drift using values $p = 0.3$ and $p = 0.8$, respectively.

Mean squared distance dependence on the number of steps It is predicted that the average squared displacement, $\langle s^2 \rangle$, for an ensemble of independent particles following a simple random walk should be proportional to the number of steps, n, taken by the ensemble of particles. This hypothesis was tested by simulating random walk paths for many different amounts of steps taken using Monte Carlo trials with 1,000 paths per value for n. With this data, the mean distance travelled was plotted against the square root of the number of steps taken.

2D and 3D extensions of the random walk model Extending the simulations of a one-dimensional random walk to higher dimensions provides a qualitative depiction of Brownian motion acting on particles.

Since the one-dimensional simple random walk model is based on uniform random movement along one dimension, the higher dimensional models simulated were also taken to depend on uniformly random variables, albeit described by continuous probability distributions instead of a discrete distribution.

To model a single 2D random walk step, a uniform random float in the interval $[0, 1]$ was generated, then multiplied by 2π. This random value, denoted θ, is the angle describing the direction of the step, and could be used to describe the vector of movement in polar coordinates. The Cartesian coordinates for each step could be found by transforming the polar coordinates given by $x = rcos\theta$, $y = rsin\theta$, where r is the step size. The step size, r, was set to unity when modelling 2D random walk steps. The full path traced by a single random walk in 2D was simulated by adding each step. To illustrate qualitatively the behaviour of this process, a sample of random paths was plotted for the 2D random walk model using Python.

To model a 3D random walk step, the same procedure for finding a uniform random angle, theta, was done as in the 2D random walk to generate the direction of motion along the x-y plane. However, an extra z-component was required. The z-component was found by generating a uniformly random variable between $[-1, 1]$. The 3D model thus used two independent random variables. This method is valid however, since both random variables used are uniformly random. With an angle θ on the x-y plane and a z-coordinate, the resultant vector for a single step could be found by converting polar coordinates to Cartesian coordinates using the following transformations: $z = z$, $x = \alpha cos\theta$, $y = \alpha sin\theta$, where $\alpha = \sqrt{1 - z^2}$ was used to ensure the magnitude of each step was unity. To illustrate qualitatively the behaviour of this process, a sample of random paths was plotted for the 3D random walk model using Python.

3.1.2 Arithmetic and geometric Brownian motion simulations

The aim of this section was to determine if the theoretical solutions can accurately predict the mean and variance of arithmetic and geometric Brownian motion in practice. To conduct this comparison, the constants μ and σ were first isolated in terms of the expected value, variance and time elapsed, using the theoretical mean and variance expressions resulting from the exact solution of each model. By retrieving statistical data on the random simulations of these models, the resulting parameters μ and σ were determined, and hence allowed for verification of whether or not the theoretical mean and variance values match.

Arithmetic Brownian motion comparison Using the fact that $dx = x(t+dt) - x(t)$, the equation for arithmetic Brownian motion, Eq. (2.18), can be rewritten in discrete form if the transformations $x(t) \to x_i$ and $x(t+dt) \to x_{i+1}$ are used, giving the following:

$$x_{i+1} = x_i + \mu dt + \sigma\sqrt{dt}N(0,1),\ i = 0, 1, 2, ..., n \tag{3.1}$$

Using Eq. (3.1), arithmetic Brownian motion could then be modelled computationally in Python.

By Eq. (2.19), one can easily solve for μ and σ after time Δt:

$$\mu = \frac{E\left[x(t)\right] - x(0)}{\Delta t} \qquad |\sigma| = \sqrt{\frac{V\left[x(t)\right]}{\Delta t}} \tag{3.2}$$

which can be used with the Monte Carlo simulated expected values and variances at each time to calculate μ and σ, respectively, for comparison with theoretical results. The expressions above were used to compare the Monte Carlo trialled results for μ and σ over 10,000 trials for arithmetic Brownian motion, with a comparison done on varying the time step dt.

Geometric Brownian motion comparison As outlined in the section 2.1, the stochastic differential equation describing geometric Brownian motion is given, in terms of the natural log of the process, as,

$$\ln x(t) = \ln x_0 + \left(\mu - \frac{\sigma^2}{2}\right)\Delta t + \sigma\sqrt{\Delta t}\tilde{N} \tag{3.3}$$

where $x(t_0) = x_0$.

By using the normal distribution transformation property one ends to the following relation:

$$\ln x(t) = N\left(\ln x_0 + \left(\mu - \frac{\sigma^2}{2}\right)\Delta t, \sigma^2\Delta t\right) \tag{3.4}$$

which implies that $x(t)$ is lognormally distributed.

The expectation value and variance of the lognormal distribution above are found to be,

$$E\left[x(t)\right] = e^{\ln x_0 + \mu\Delta t} \qquad V\left[x(t)\right] = e^{2(\ln x_0 + \mu\Delta t)} \cdot \left(e^{\sigma^2\Delta t} - 1\right) \tag{3.5}$$

The above results show that for a random quantity described by geometric Brownian motion, the mean and variance grow exponentially with time for $\mu > 0$.

By Eq. (3.5), one can easily solve for μ and σ:

$$\mu = \frac{\ln E\left[x(t)\right] - \ln x_0}{\Delta t} \qquad |\sigma| = \sqrt{\frac{\ln\left(\frac{V[x(t)]}{E[x(t)]^2} + 1\right)}{\Delta t}} \tag{3.6}$$

which can be used with the Monte Carlo simulated expected values and variances at each time to calculate μ and σ, respectively, for comparison with theoretical results. As such, as with the arithmetic Brownian model, the expressions above were used to compare the Monte Carlo trialled results for μ and σ over 10,000 trials for geometric Brownian motion, with a comparison done on varying the time step dt.

Using the fact that $dx = x(t + dt) - x(t)$, the equation for geometric Brownian motion, Eq. (2.22), can be rewritten in discrete form if the transformations $x(t) \to x_i$ and $x(t + dt) \to x_{i+1}$ are used, giving the following:

$$x_{i+1} = x_i e^{\left[(\mu - \frac{\sigma^2}{2})dt + \sigma\sqrt{dt}N(0,1)\right]},\ i = 0, 1, 2, ..., n \tag{3.7}$$

Using Eq. (3.7), geometric Brownian motion was modelled computationally in order to compare the analytical and simulated results for μ and σ.

3.1.3 Ornstein-Uhlenbeck simulations

To fully explore the statistical properties of Ornstein-Uhlenbeck Brownian motion, the process was modelled using different parameters and compared. The coefficients μ and τ, as well as the time step dt were varied and their effects on the model explored. The mean squared velocity was also modelled against time to show the behaviour of the mean squared velocity in steady-state.

Using the fact that $dv = v(t + dt) - v(t)$, the equation for Ornstein-Uhlenbeck Brownian motion given Eq. (2.33) can be rewritten in discrete form if the transformations $v(t) \to v_i$ and $v(t + dt) \to v_{i+1}$ are used, giving the following:

$$v_{i+1} = v_i - \frac{1}{\tau}v_i dt + \frac{\sigma_0}{\sqrt{\tau}}\sqrt{dt}N(0,1),\ i = 0, 1, 2, ..., n \tag{3.8}$$

As such, Eq. (3.8) was used to model Ornstein-Uhlenbeck Brownian motion computationally using Python.

3.2 Investigation of FEL SASE radiation

A key outcome of this project is to computationally model the emitted radiation produced by a free-electron laser based on the analytical theory proposed by Krinsky, Li (2006)[19] based on the analysis of shot noise by Rice (1944)[16]. This section details how this was achieved. As in the previous section, the programming language used throughout was Python.

3.2.1 Modelling a temporally coherent Gaussian pulse

FEL SASE radiation without seeding is, in principle, represented by a stochastic field, and a key aim of this project is to model such radiation. However, to ensure that the approach to modelling such a field is correct, it is worth first verifying said approach with a deterministic field. As such, a quasi-monochromatic plane-wave electromagnetic field with Gaussian envelope, expressed as,

$$E_0(t) = e_0 e^{\left(-\frac{t^2}{4\sigma_\tau^2} + i\omega_r \tau\right)} \tag{3.9}$$

was modelled in the time domain, using two sets of parameters $\sigma_\tau = 2, \omega_r = 3$ and $\sigma_\tau = 1, \omega_r = 3$, where σ_τ is defined as the RMS temporal width of the intensity profile $|E_0(t)^2|$, and ω_r is the resonance frequency of the pulse. The expected result produced by this simulation is a plot of two symmetrical Gaussian pulses centred about 0, with the pulse with larger σ_τ having a wider spread.

For a deterministic Gaussian pulse, the coherence time is given by $t_{coh} = 2\sigma_\tau\sqrt{\pi}$. To verify the approach used for the calculation of coherence time in the general sense, it was first calculated for a coherent pulse. The expected coherence time for a coherent pulse with Gaussian envelope with parameters $\sigma_\tau = 2, \omega = 3$ is equal to $\cong 7.0898$.

It should be noted that in the calculation of autocorrelation for a deterministic pulse, a sample average was not required since by definition the variance of results is zero, and hence the autocorrelation was done using values of a single trial.

The intensity profile for a temporally coherent Gaussian pulse was also modelled in the time domain. The expected result of this is to see a normal distribution centred on 0. There should be a single (central) mode.

By taking the Fourier transform of the electric field of a radiation pulse, one attains its frequency spectrum. For a coherent pulse, the frequency profile of the electric field is analytically given by,

$$E_0(\omega) = \int E_0(t) e^{-i\omega t} dt = \frac{e_0\sqrt{\pi}}{\sigma_\omega} e^{\left[-\frac{(\omega-\omega_r)^2}{4\sigma_\omega^2}\right]} \tag{3.10}$$

where $\sigma_\omega = \frac{1}{2\sigma_\tau}$ is the RMS width of the frequency profile $|E_0(\omega)|^2$.

Using the temporal electric field profile for a coherent Gaussian-envelope pulse, a discrete Fourier transform was taken for all points and plotted. To validate the robustness of this approach, the analytical frequency spectrum (as described above) was plotted for comparison.

3.2.2 Modelling a pulse with uniform arrival time probability density profile

When the arrival time t_j is a uniformly distributed random variable, the output radiation of the FEL pulse can be described by a shot noise process. The instantaneous electronic current density at time t is represented as a discrete pulse train, given by $j_e = -\sum_j \delta(t - t_j)$. The average electronic current density, $\langle j_e(t) \rangle$ can be found only when the behaviour of t_j is known.

To investigate the shot noise current contribution for a uniformly random electron bunch density, a simplified version of the pulse was modelled. Disregarding all contributions except for $\sum_{j=1}^{N_e} e^{-(t-t_j)^2}$, the radiation for the pulse was simulated in the time domain.

It was expected that since the value to be taken as a negative exponent, $(t-t_j)^2$, is uniformly distributed, the sum of many random terms should be independent of t for $-\frac{T}{2} < t < \frac{T}{2}$. The shape of this pulse should approach a square wave, with $\langle E(t) \rangle = \mu$ being time-invariant inside the bunch length limits.

The expectation value for this square wave was found analytically using elementary probability theory. For a pulse with bunch length T and number of sources N_e, the expected value for $E(t)$ within $\left[-\frac{T}{2}, \frac{T}{2}\right]$ is given by

$$\langle E(t) \rangle = \frac{N_e\sqrt{\pi}}{T} \tag{3.11}$$

The above expression allows for predictions of the average E-field to be tested computationally. This was done using Monte Carlo trials for different values of T and N_e. The derivation for Eq. (3.11) is given in the appendix.

The analytical expression for the average intensity is not found trivially, since its evaluation depends on the square of a sum of random variables. As such, an analytical expression for the time averaged intensity is not presented in this paper. However, it is still predicted that the intensity should demonstrate the same square pulse behaviour. This prediction was tested using Monte Carlo simulations.

3.2.3 Modelling a pulse with Gaussian arrival time probability density profile

When the arrival time t_j follows a Gaussian distribution, the output radiation of the FEL pulse is no longer time-invariant, since $(t - t_j)^2$ is itself not uniformly distributed. As with the case of a uniform bunch density, to investigate the shot noise current contribution with a Gaussian random electron bunch density, a simplified version of the pulse was modelled. Disregarding all contributions except for $\sum_{j=1}^{N_e} e^{-(t-t_j)^2}$, the radiation for the pulse was simulated in the time domain. The electron bunch density used was the following Gaussian:

$$f_{t_j}(t) = \frac{1}{\sigma_e\sqrt{2\pi}} e^{-\frac{t^2}{2\sigma_e^2}} \tag{3.12}$$

where σ_e is the standard deviation in the electron bunch. It is expected that this pulse's electric field and intensity should exhibit Gaussian behaviour about t= 0. This prediction was tested using Monte Carlo trials for different values of σ_e and N_e.

3.2.4 FEL SASE radiation with uniform electron bunch density profile

The full expression for SASE radiation emission as in Eq. (2.49) was modelled in the time domain. The electric field and intensity profiles were plotted in the time domain both for a single shot, and using Monte Carlo trials over 500 trials. This was done to contrast the statistical profile of a single pulse against that of a large sample of such pulses. It is predicted that the electric field should go to zero for all t when averaged over a large number of samples, due to the cosine term in the real expression for the electric field.

The average intensity of the radiation as a function of the number of electrons in the bunch, N_e, was explored by conducting Monte Carlo trials of many samples of pulses for different values of N_e and plotting the results. This was done for the uniform electron bunch density case, but, in principle, performing the same test on the Gaussian bunch density case would demonstrate the same relationship, given that the intensity is evaluated at a consistent time t for each trial.

A quantity of key statistical importance in ascertaining the characteristics of a stochastic process is its autocorrelation function. Using the normalised autocorrelation as in Eq. (2.54), the time invariance of the process was tested. This was done by taking the normalised autocorrelation at $t = 0$ and $t = 10$ for an ensemble of 500 sample simulated pulses. In principle, the same simulated electric field data should be used for the determination of these two autocorrelation profiles. In practice, this was done using two different samples of trialled electric field data. However, the analysis should be approximately the same since the radiation being modelled is ergodic.

The power spectral density (PSD) was attained for simulated SASE radiation with uniform electron bunch density by taking the Fourier transform of the autocorrelation function (for autocorrelation at $t = 0$). The resonance frequency used for the simulated FEL pulse was $\omega_r = 6$. It is predicted that there should be a peak at this resonance frequency in magnitude spectrum. In taking the Fourier transform of the autocorrelation, the phase spectrum of the PSD was also attained and plotted. It is predicted that the phase should be zero at the resonance frequency.

3.2.5 FEL SASE radiation with Gaussian electron bunch density profile

The full expression for SASE radiation emission as in Eq. (2.51) was modelled in the time domain. The electric field and intensity profiles were plotted in the time domain both for a single shot, and using Monte Carlo trials over 500 trials. This was done to contrast the statistical profile of a single pulse against that of a large sample of such pulses. As with the uniform bunch density case, it is predicted that the electric field should go to zero for all t when averaged over a large number of samples.

Using the normalised autocorrelation as in Eq. (2.54), the time invariance of the process was tested. This was done by taking the normalised autocorrelation at $t = 0$ and $t = 10$ for an ensemble of 500 sample simulated pulses.

The power spectral density (PSD) was attained for simulated SASE radiation with Gaussian electron bunch density by taking the Fourier transform of the time-averaged autocorrelation function as in Eq. (2.53), as opposed to the time-dependent autocorrelation as used in previous tests, since a Gaussian pulse is not time invariant. The resonance frequency used for the simulated FEL pulse was $\omega_r = 6$. It is predicted that there should be a peak at this resonance frequency in the magnitude spectrum. In taking the Fourier transform of the autocorrelation, the phase spectrum of the PSD was also attained and plotted. It is predicted that the phase should be zero at the resonance frequency.

4 Results and analysis

4.1 Brownian motion models

4.1.1 Random walk simulations

The results of the random walk simulations conducted are presented in this section. Sample one-dimensional random walks were simulated over 10 trials. Their paths are shown here:

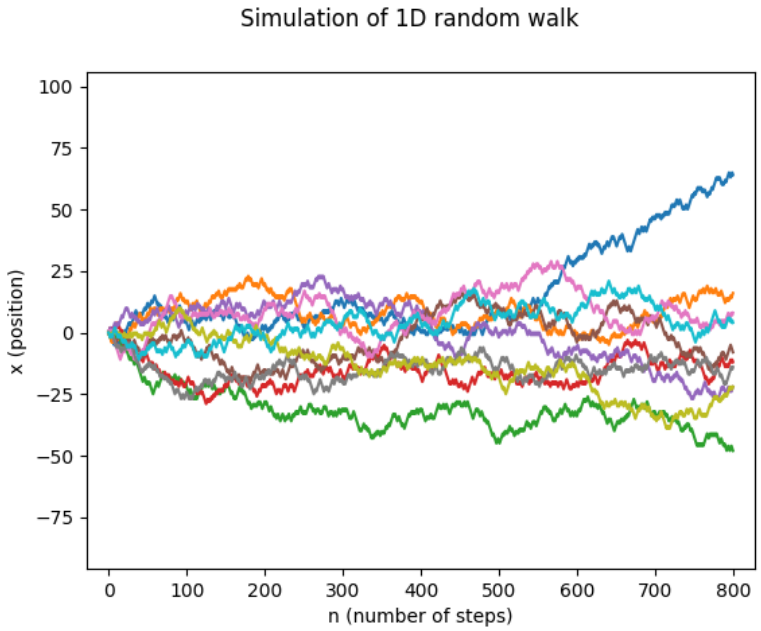

Figure 1: 10 random walk paths with no drift ($p = 0.5$), over 800 steps

The paths taken are stochastic – the final position of a random walk after 800 steps can not be predicted exactly. This is seen in figure 1 where 10 independent random walks all have different end positions despite having the same starting conditions.

Variation of the number of trials taken Next, the effect of varying the number of Monte Carlo trials taken over each simulation on the frequency distribution of final particle positions was investigated. Below can be seen the probability mass function plotted for the binomial distribution describing a random walk with parameters $p = 0.5$, $n = 800$. This is the ideal distribution for this process, and as such can be used qualitatively for comparison with the simulated results.

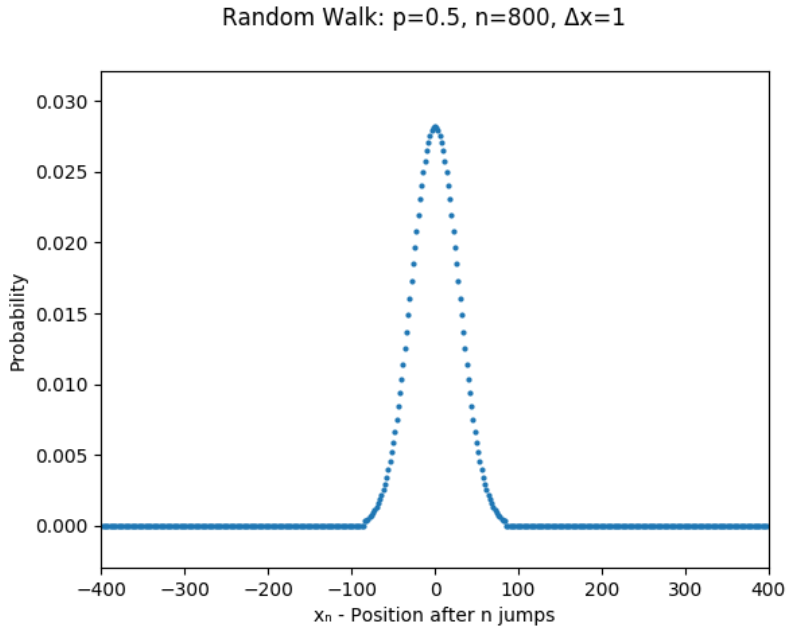

Figure 2: Analytical probability mass function describing a simple random walk ($p = 0.5$, $n = 800$)

Keeping the drift and number of steps constant, the number of Monte Carlo trials conducted was varied. The frequency distributions and histograms of the final positions are presented below, for 40, 1,000 and 1,000,000 trials.

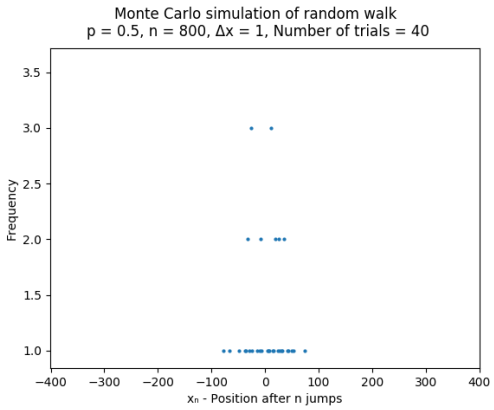

(a) Frequency distribution, 40 trials

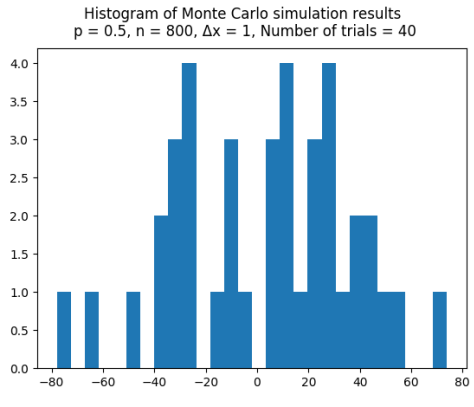

(b) Histogram, 40 trials

Figure 3: Frequency distribution (a) and histogram (b) of the final positions over 40 trials

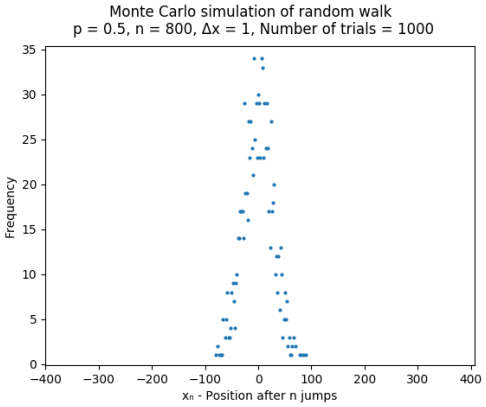

(a) Frequency distribution, 1,000 trials

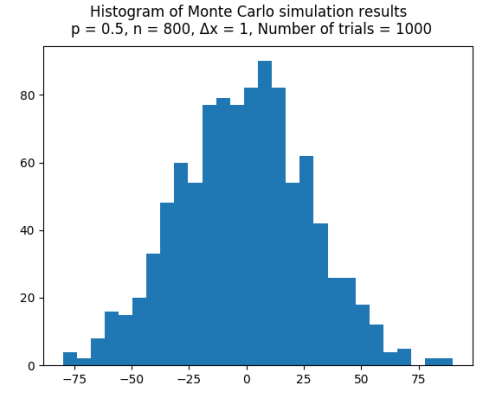

(b) Histogram, 1,000 trials

Figure 4: Frequency distribution (a) and histogram (b) of the final positions over 1,000 trials

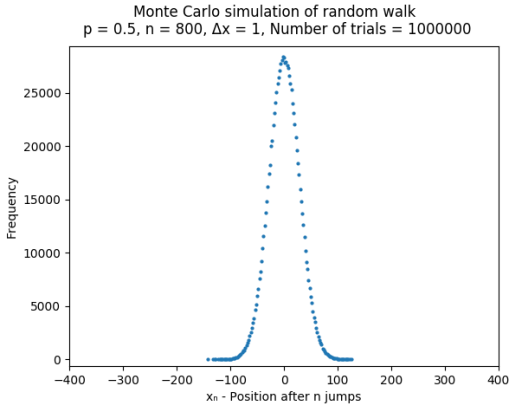

(a) Frequency distribution, 1,000,000 trials

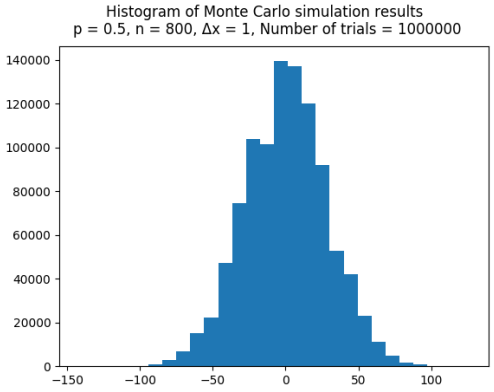

(b) Histogram, 1,000,000 trials

Figure 5: Frequency distribution (a) and histogram (b) of the final positions over 1,000,000 trials

From figures 3-5 above, a clear relationship can be seen between the number of trials and how well the frequency distribution fits the analytical probability distribution. Using 1,000,000 trials demonstrates a very close approximation to the analytical distribution in figure 2. By reducing the number of trials, it can be qualitatively observed that the frequency distributions contain more noise and appear increasingly less continuous.

These simulations also produced the mean and variance found for each ensemble of paths, which provided a quantitative means in which to investigate the effect of varying the number of trials. The mean and variance values found from the ensemble paths are compared with the mean and variance values of the binomial distribution of the same parameters, given as $\mu = 0$, $\sigma^2 = 800$. The ensemble mean and variance values and relative errors are presented in table 1 below. Since the predicted average of the final position is at $x = 0$, the error for μ is given in units of the predicted standard deviation $= \sqrt{800}$, since the distribution is Gaussian.

	μ	σ^2
Predicted value	0	800
Result found in simulations	2.050	842.3
Error between predicted result	0.0724σ	5.288%

(a) Results found for μ and σ^2 over 40 Monte Carlo trials.

	μ	σ^2
Predicted value	0	800
Result found in simulations	0.9541	803.8
Error between predicted result	0.0337σ	0.475%

(b) Results found for μ and σ^2 over 1,000 Monte Carlo trials.

	μ	σ^2
Predicted value	0	800
Result found in simulations	0.0067	797.3
Error between predicted result	$2.368 \times 10^{-4}\sigma$	-0.3375%

(c) Results found for μ and σ^2 over 1,000,000 Monte Carlo trials.

Table 1: Results found for μ and σ^2 for 40 (a), 1,000 (b) and 1,000,000 (c) trials

By comparison of the values of μ and σ^2 in table 1, it's seen that the accuracy of results increases as the number of trials is increased. This demonstrates ergodicity for the random walk model – a sufficiently large sample is shown to represent the overall statistical properties of the process.

Notable in the above results is the diminishing accuracy gain of σ^2 as the number of trials is increased. Increasing the number of trials by a factor of 25, from 40 trials to 1,000, leads to a reduction of error in σ^2 to 0.09 of the 40 trial calculation. However, increasing the number of trials by a factor of 10^3, from 1,000 to 1,000,000 will leads to a reduction of error in σ^2 to 0.71 of the 1,000 trial calculation. This diminishing return in accuracy is not observed in the mean calculations. Increasing the number of trials from 40 to 1,000 leads to a reduction of error in μ to 0.47 of its 40 trial calculation, but increasing the number of trials from 1,000 to 1,000,000 leads to a reduction of error in μ to 0.007 of the 1,000 trial calculation, which is a significant increase in accuracy.

Variation of drift parameter Next, the results of varying the drift parameter, p, were investigated. In principle, any drift parameter that isn't centred ($p = 0.5$) leads to an overall drift in the direction of motion, leading to the average final position that's different from the initial position. To explore the effect of varying this parameter, 10 sample random paths were plotted to illustrate the qualitative effect and the statistical properties were obtained for 10,000 Monte Carlo trials, using drift parameter values of $p = 0.3$ (leftward drift) and $p = 0.8$ (rightward drift). The frequency distributions of these Monte Carlo trials were then plotted, and values for μ and σ^2 were compared with the theoretically predicted values.

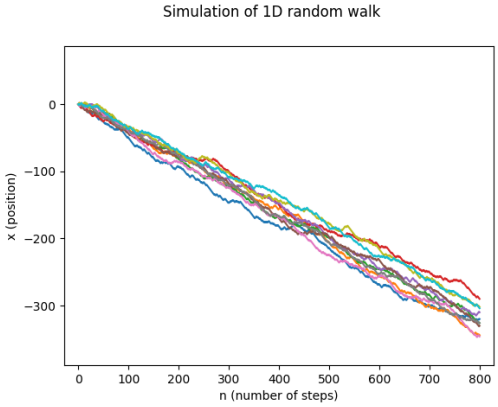

(a) Random walk, $p = 0.3$

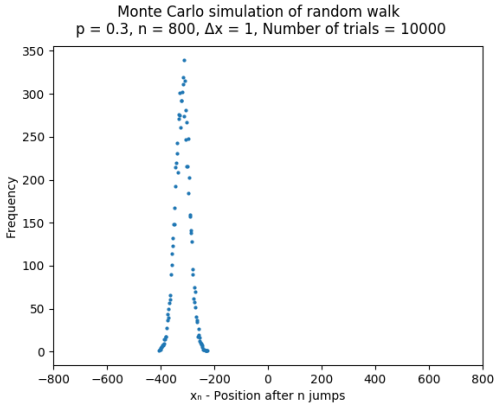

(b) Frequency distribution, $p = 0.3$

Figure 6: 10 sample random paths (a) and frequency distribution of the final positions over 10,000 trials (b) for a random walk with drift parameter $p = 0.3$ (leftward drift). Number of steps taken $n = 800$.

(a) Random walk, $p = 0.8$

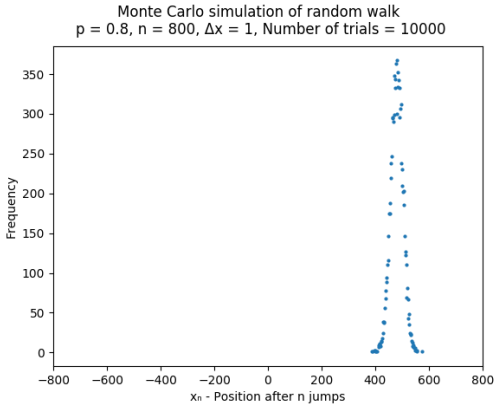

(b) Frequency distribution, $p = 0.8$

Figure 7: 10 sample random paths (a) and frequency distribution of the final positions over 10,000 trials (b) for a random walk with drift parameter $p = 0.8$ (rightward drift). Number of steps taken $n = 800$.

The ensemble mean and variance values and relative errors are presented in table 2 below.

	μ	σ^2
Predicted value	-320	672
Result found in simulations	-320.065	682.47
Error between predicted result	-0.02%	-1.56%

(a) Results found for μ and σ^2 for drift parameter $p = 0.3$

	μ	σ^2
Predicted value	480	512
Result found in simulations	480.162	499.59
Error between predicted result	0.03%	2.42%

(b) Results found for μ and σ^2 for drift parameter $p = 0.8$

Table 2: Results found for μ and σ^2 for $p = 0.3$ (a), and $p = 0.8$ (b) over 10,000 trials

As can be seen from figure 6a, when $p < 0.5$, the paths tend to drift negatively with respect to the starting position, and from 6b it's seen that the paths drift positively when $p > 0.5$. The effect of this drift on the frequency distributions of the end positions is a linear transformation of the final position, left of the initial position for $p < 0.5$ and right of the initial position for $p > 0.5$, as shown in figure 7a and 7b, respectively. Table 2 give the expected and simulated mean and variance values for the random walks. A low error in the trialled mean values are found in comparison with the predicted values, confirming that the simulations agree with theoretical binomial distribution model for the random walks. A sufficiently low error in the trialled variance values are found in comparison with the predicted variances, but it is found that the error in variance for trialled random walks is higher than that for a driftless random walk, since relative error in variance is greater when drift is included for the 10,000 trial Monte Carlo runs, compared to a lower variance in error for only a 1,000 Monte Carlo trial simulation for the non-drifted random walk.

Mean squared distance dependence on the number of steps Theoretically, the mean squared distance of a random walk taken by a particle is proportional to the number of steps taken. To test this hypothesis, the mean distance from the initial position after n steps was found using 1,000 Monte Carlo trials for different values of n, with drift parameter set to $p = 0.5$. 1,000 trials were used in this simulation, since, for large numbers of steps, testing this dependence becomes very computationally expensive. With this trialled data, the mean distance s was plotted against $\sqrt{n}$.

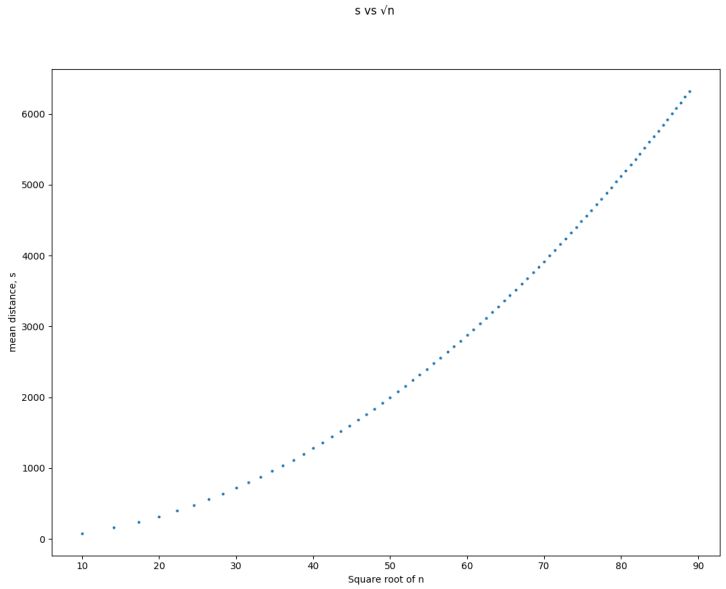

Figure 8: Mean distance of final position vs $\sqrt{n}$ over 1,000 trials for driftless random walk simulations.

Figure 8 shows the mean distance as a function of $\sqrt{n}$. It is seen that for lower values of n ($\sqrt{n} < 60$) the relationship is nonlinear, resembling a quadratic dependence of the mean distance on $\sqrt{n}$). As n increases however, a linear relationship is seen between s and $\sqrt{n}$, which is the theoretical proportionality result expected.

2D and 3D extensions of the random walk model A sample of 50 random paths drawn for the 2D random walk was drawn. Two methods of visual representation were used to show the paths taken – an x-y phase diagram was plotted, which shows the paths taken on a 2D projection across all time, and a 3D plot of the 2D positions as a function of time was drawn.

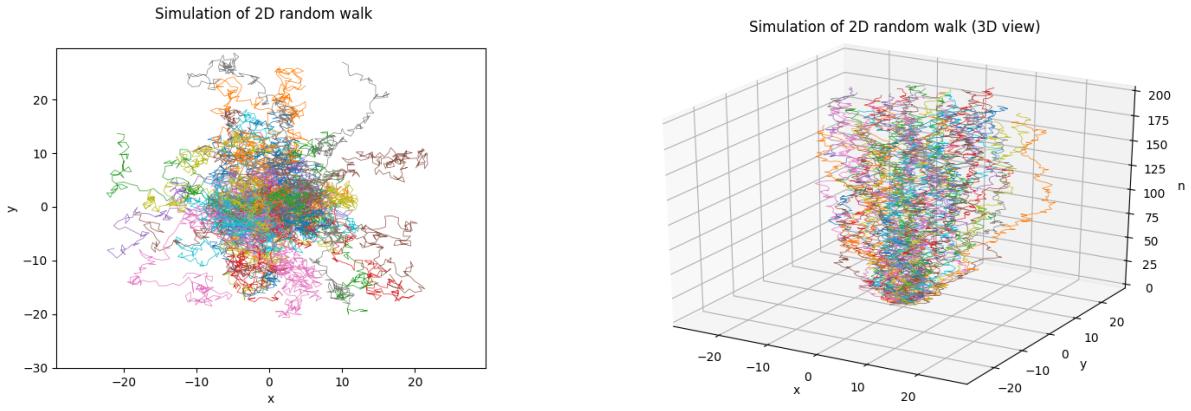

(a) 2D random walk, phase space

(b) 2D random walk, shown in 3D view plotted against time

Figure 9: 2D random walk trajectories plotted in x-y phase space (a) and as a function of time (b)

As can be seen from the phase diagram in figure 9a, the mean position of the path is approximately at

$(0, 0)$ since the average reach of the path extends outwards approximately isotropically from the centre. Figure 9b shows the 2D paths traced as a function of time. The side profile of the paths against time resembles a one-dimensional random walk sample, even though this is a random walk in 2D space.

A sample of 50 random paths drawn for the 3D random walk was drawn. A 3D phase diagram of the trajectories taken was plotted.

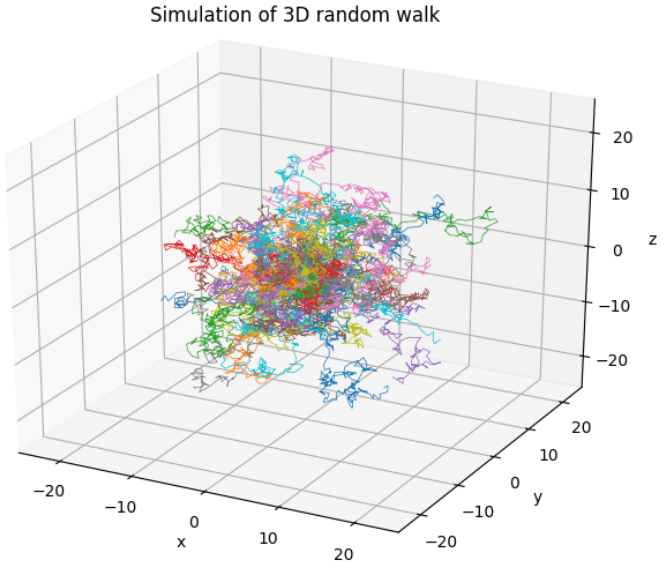

Figure 10: 3D random walk trajectories plotted in three-dimensional phase space

Although qualitatively less clear the 1D and 2D random walk plots, the 3D phase space diagram in figure 10 demonstrates that the mean position of the path is approximately at $(0, 0, 0)$, since the average reach of the path extends approximately outwards isotropically.

4.1.2 Arithmetic and geometric Brownian motion simulations

Arithmetic Brownian motion results Using Python, a Monte Carlo script was written to simulate arithmetic Brownian motion (ABM). Figure 11 shows a simulation of ABM, with 30 trials being displayed.

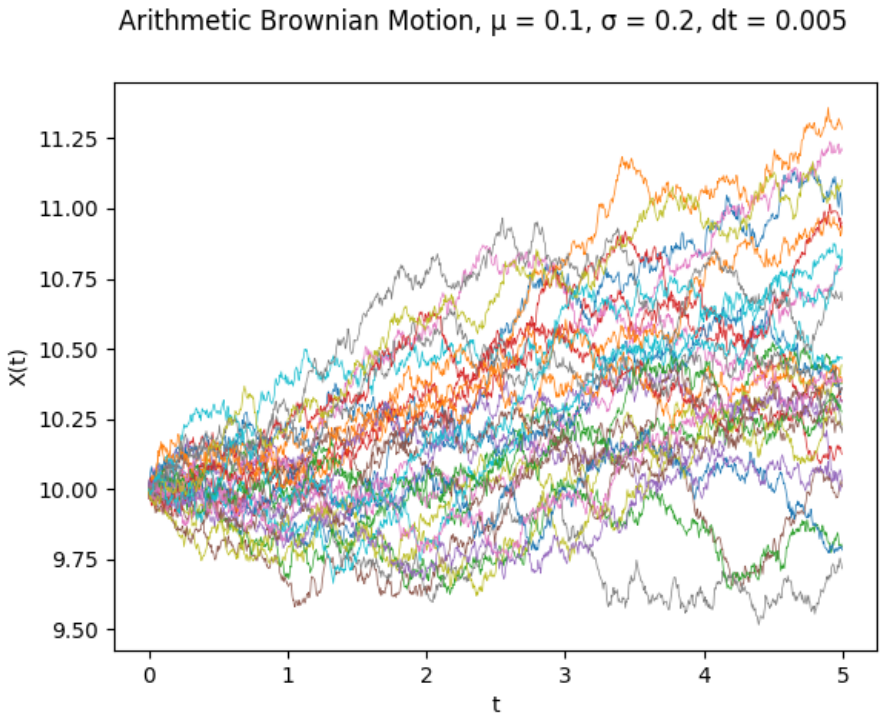

Figure 11: Simulation of arithmetic Brownian motion. 30 trials shown

To attain precise values for μ and σ, the number of Monte Carlo trials was set to 10,000. Maximum time elapsed was set at 5 seconds. To explore the effect of step size dt, two different values were used; $dt = 0.01$ and $dt = 0.005$.

The results of these simulations can be seen in table 3 and table 4. The results are very close to the theoretical values for μ and σ, but fall outside the 95% confidence interval for the sample of 10,000 trials. This is the case for both values of dt used.

It was expected that a smaller step size would produce results closer to the theoretical ones. This turned out not to be the case. In practice, the relative error for μ was more than 11 times greater for the smaller dt value, and the relative error for σ was found to be a factor of 1.5 greater for the smaller dt value. It should still be stated however that the error in σ is still qualitatively very low for both trials can be considered to be quite an accurate result, given the process is pseudo-random.

	μ	σ
Predicted value	0.1	0.2
Average value found	0.1003	0.2001
95% CI margin of error in results	5.1×10^{-5}	10^{-5}
95% confidence interval range	$[0.10020, 0.10033]$	$[0.20011, 0.20013]$
Relative error from predicted result	0.28%	0.0616%

Table 3: Monte Carlo-determined values for μ and σ for arithmetic Brownian motion over 10,000 trials. $dt = 0.01$

	μ	σ
Predicted value	0.1	0.2
Average value found	0.0969	0.1998
95% CI margin of error in results	3.6×10^{-5}	2.4×10^{-5}
95% confidence interval range	$[0.0968, 0.09691]$	$[0.19979, 0.19984]$
Relative error from predicted result	3.13%	0.09%

Table 4: Monte Carlo-determined values for μ and σ for arithmetic Brownian motion over 10,000 trials. $dt = 0.005$

Geometric Brownian motion results Using Python, a Monte Carlo script was written to simulate geometric Brownian motion (GBM). Figure 12 shows a simulation of GBM, with 60 trials being displayed.

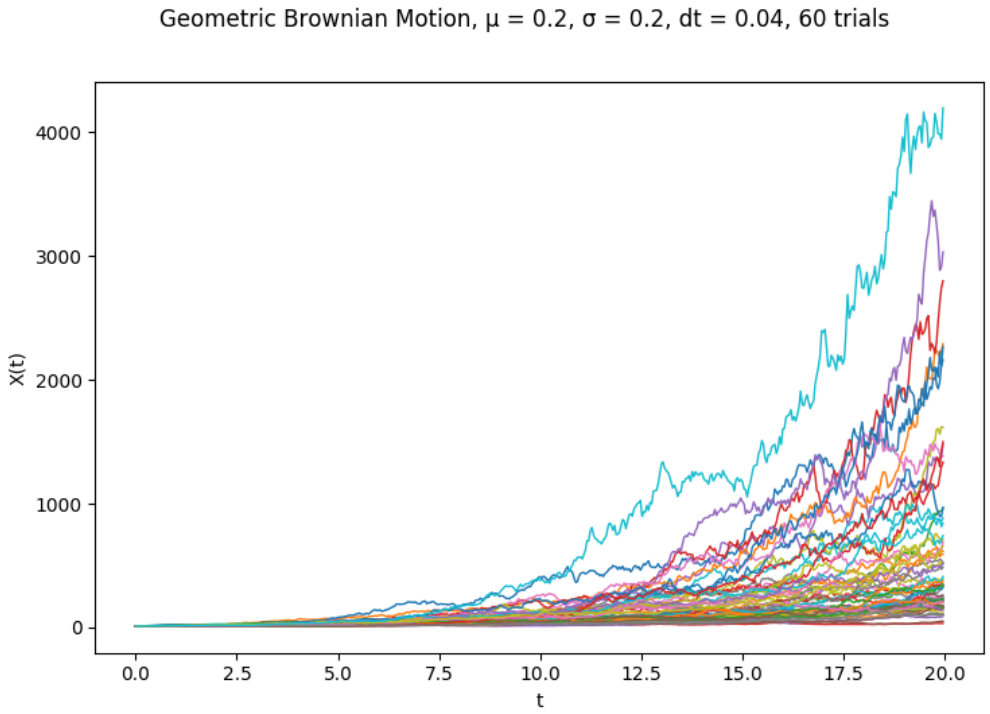

Figure 12: Simulation of geometric Brownian motion. 60 trials shown

As with the ABM simulations, the number of Monte Carlo trials was set to 10,000 and maximum time elapsed was set at 5 seconds. To explore the effect of step size dt, two different values were used; $dt = 0.01$ and $dt = 0.005$.

The quantitative results of these simulations can be seen in table 5 and table 6. The results are very close to the theoretical values for μ and σ, but, much like the ABM simulations, fall short of the 95% confidence interval for the sample of 10,000 trials. This is the case for both values of dt used.

The relative error for μ was 2.48 times greater for the smaller dt value, and the relative error for σ was found to be *smaller* when testing with the lower dt value, unlike with the ABM trials. Much like the ABM trials, the percentage error in σ is significantly lower than that of μ in both cases.

	μ	σ
Predicted value	0.05	0.1
Average value found	0.04974	0.10002
95% CI margin of error in results	2.9×10^{-5}	8×10^{-6}
95% confidence interval range	$[0.04871, 0.04977]$	$[0.09997, 0.09999]$
Relative error from predicted result	0.52%	0.02%

Table 5: Monte Carlo-determined values for μ and σ for geometric Brownian motion over 10,000 trials. $dt = 0.01$

	μ	σ
Predicted value	0.05	0.1
Average value found	0.0506	0.10001
95% CI margin of error in results	1.2×10^{-5}	10^{-5}
95% confidence interval range	$[0.05063, 0.05065]$	$[0.09997, 0.09999]$
Relative error from predicted result	1.29%	0.01%

Table 6: Monte Carlo-determined values for μ and σ for geometric Brownian motion over 10,000 trials. $dt = 0.005$

Analysis This subsection has provided a comparison between the theoretical and simulated mean and standard deviation values for both ABM and GBM by comparing the parameters μ and σ. Although the trials showed results that were very close, there wasn't a single observed case of the Monte Carlo 95% confidence intervals for μ or σ that included the theoretical values, despite using a large sample size of $n = 10,000$. Hence, these results alone do not rigorously prove that the simulated and theoretical values match.

To improve on this setup with the aim to show that simulated mean and standard deviation values agree with the theory, more comprehensive simulations could be conducted. The number of trials could be increased from $n = 10,000$ to, say, $n = 1,000,000$ and the time elapsed could be increased from 5 seconds up to 500 seconds. This would provide a sufficiently large sample from which to draw data from. The scripts provided in the appendix are ill-equipped to accomplish this - in order to conduct such simulations one would be required to employ heavy parallelization to run the Monte Carlo trials in a sufficiently short period of time. This is the next step for improving on this comparison.

4.1.3 Ornstein-Uhlenbeck Brownian motion

The results of the Ornstein-Uhlenbeck simulations conducted are presented in this section. Taking a single path described by Ornstein-Uhlenbeck Brownian motion, using parameters $v_0 = 0$, $\tau = \sigma = 1$, $dt = 0.001$, produces the characteristic white noise signal in the time domain shown in figure 13. This section details the results for the investigation of statistical properties of this stochastic process with variation of parameters dt, τ, σ. The results for the steady-state mean squared velocity of a particle described by this process are presented in this section also.

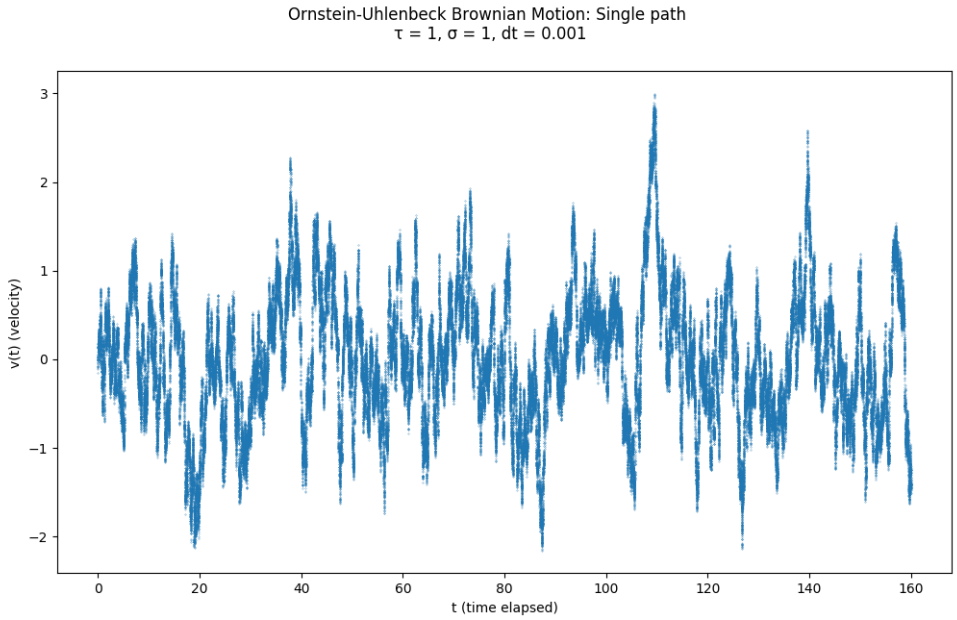

Figure 13: A single run of Ornstein-Uhlenbeck Brownian motion (white noise signal) over 160 units of time. This path can be used to describe the velocity of a particle in a fluid undergoing thermal fluctuations based on the Ornstein-Uhlenbeck stochastic process.

Variation of time step size The effect of varying the step size dt on the behaviour of Ornstein-Uhlenbeck Brownian motion was modelled. Values of dt used were 0.001 and 10^{-4}. The average velocity as a function of time was plotted over 100 Monte Carlo simulations along with the standard deviation as a function of time.

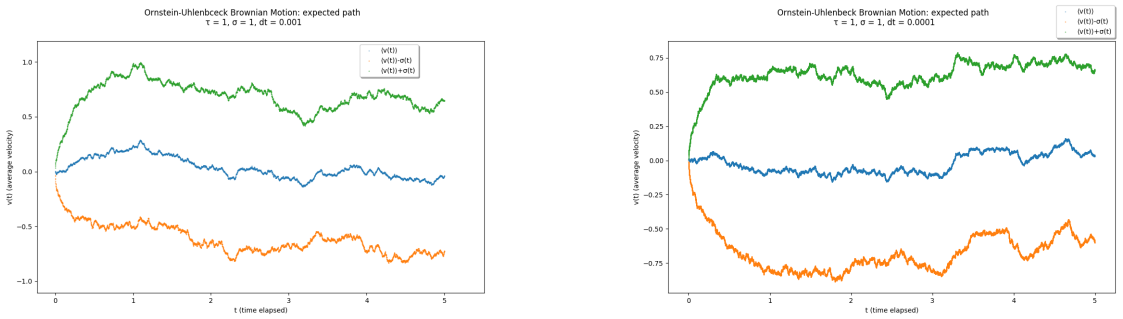

(a) $\langle v(t) \rangle \pm \sigma(t)$ over 100 independent Ornstein-Uhlenbeck runs, using $dt = 0.001$

(b) $\langle v(t) \rangle \pm \sigma(t)$ over 100 independent Ornstein-Uhlenbeck runs, using $dt = 10^{-4}$

Figure 14: Monte Carlo averaged path taken by 100 independent Ornstein-Uhlenbeck runs, using $dt = 0.001$ (a) and $dt = 10^{-4}$ (b). Also plotted is the standard deviation added and subtracted for each point $\langle v(t) \rangle$.

From figure 14 it is seen that reducing dt by a factor of 10 has no effect on the behaviour of the average process. Ornstein-Uhlenbeck Brownian motion is shown to look the same at all timescales.

Demonstrating the white noise limit By using the parameters $\sigma = 1,000$, $\tau = 0.001$, the white noise limit of Ornstein-Uhlenbeck Brownian motion was tested, using a simulated average of 100 independent Monte Carlo trials. This is shown in figure 15.

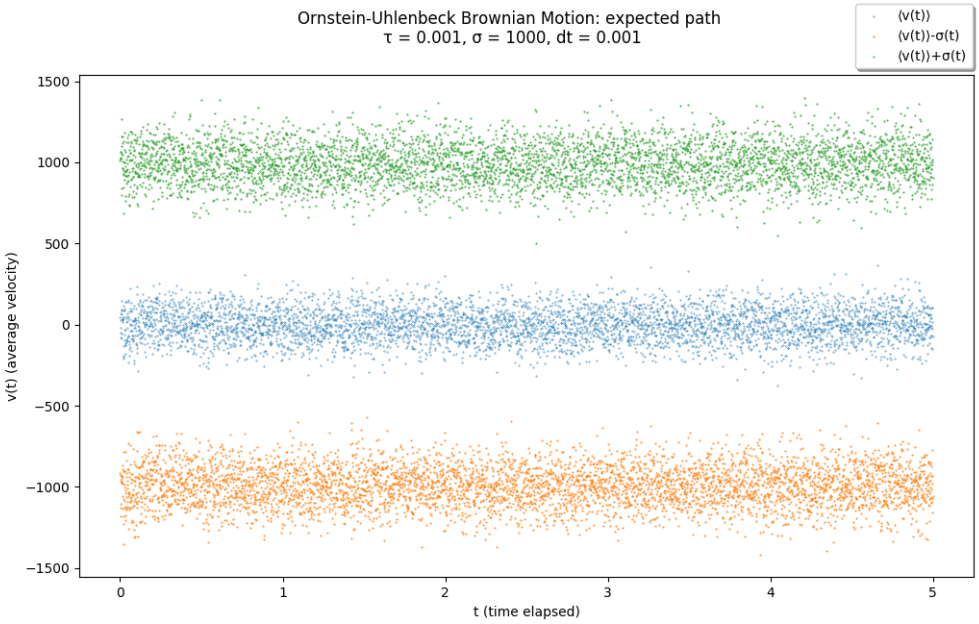

Figure 15: Plot of $\langle v(t) \rangle \pm \sigma(t)$, using OU paramters $\tau = 0.001$ and $\sigma_0 = 1,000$

It can be seen from figure 15 that every point $\langle v(t) \rangle$ is time-invariant and independently random (caused by the high variance $\sigma^2 = 10^6$), since there appears to be no time-dependent relationship between points. Along with this observation, the expected value of velocity $\langle v(t) \rangle = 0 \; \forall t$, which implies that the autocorrelation for this process is given by

$$R_v(t') = \langle v(t)v(t-t') \rangle = 0, \; t' \neq 0 \tag{4.1}$$

The autocorrelation at $t' = 0$ is given by $R_v(0) = \left\langle v(t)^2 \right\rangle = \sigma^2$, since the mean is always 0. Thus, in general, the autocorrelation function for this process can be expressed as,

$$R_v(t') = \sigma^2 \delta(t - t') \tag{4.2}$$

which is the characteristic autocorrelation of white noise.

Mean squared velocity of an OU particle in steady-state According to Eq. (2.35), a particle in a fluid with speed described by Ornstein-Uhlenbeck Brownian motion will, on average, have a constant momentum in steady-state ($t \to \infty$), given by $\left\langle v^2 \right\rangle_{eq} = \frac{D\tau}{2}$,where D is the diffusion coefficient for the system. This hypothesis was tested by modelling the mean squared velocity as a function of time, using a sample of 100 independent random paths described by the Ornstein-Uhlenbeck process. Parameters used in this test were $\tau = 0.5$, $\sigma = 5$, $dt = 0.001$. The expected steady-state value for the mean squared velocity with these parameters is found to be $\left\langle v^2 \right\rangle_{eq} = 6.25$. The result of this test is given in figure 16 below.

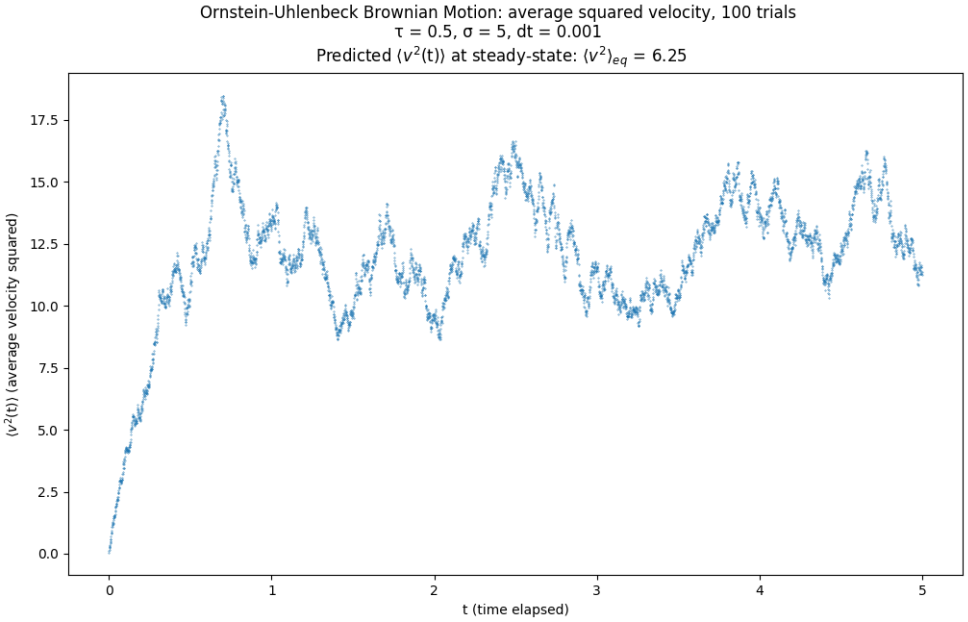

Figure 16: Mean squared velocity vs time elapsed for an ensemble of 100 independent trials of OU Brownian motion

As can be seen from figure 16, the mean squared velocity does settle to a (fairly) constant level in steady-state. There are still fluctuations in the steady-state due to the random nature of the process. One may assume that conducting this test with a far higher number of Monte Carlo trials would produce a smoother result. As such, this points to a source of improvement on the results presented.

The magnitude of the result for mean squared velocity does not agree with the analytical prediction, however. It is incorrect by a factor of 2; it is seen that in steady-state, $\langle v^2 \rangle$ fluctuates about ~ 12.5. This discrepancy could be an error in the algorithm used when modelling, or, if this is not the case, the discrepancy could be due to an ill definition of the diffusion coefficient D, in which case the analytically predicted result for the mean squared velocity as a function of time is not correct.

4.2 FEL SASE radiation simulation results

4.2.1 Modelling a temporally coherent Gaussian pulse

Pulse in time domain A coherent Gaussian pulse was modelled using parameters $\sigma_\tau = 1, 2$ and $\omega_r = 3$, and is shown in figure 17 below.

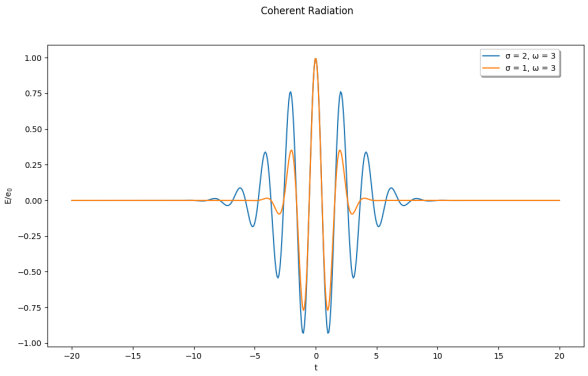

Figure 17: 2 coherent Gaussian pulses with parameters $\sigma_\tau = 1, 2$ and $\omega_r = 3$

As seen from figure 17, the pulses are centred about $t = 0$. Since the frequency of both pulses are the same, the pulses are exactly in phase. The standard deviation parameter, σ, is seen to correspond with how rapidly the pulse decays over time - the pulse with $\sigma = 2$ decays far slower than the pulse with $\sigma = 1$.

Pulse in frequency space The electric field profile of this pulse in frequency space was attained by applying the fast Fourier transform algorithm to the electric field data in the time domain. This is shown in figure 18. To verify the robustness of this approach, the analytically known Fourier transform was also plotted in figure 18.

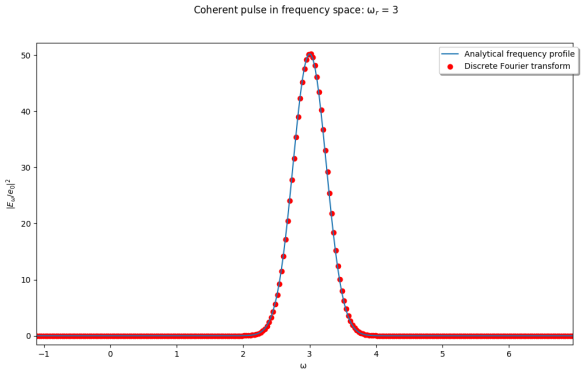

Figure 18: Analytical Fourier transform and discrete Fourier transform of coherent Gaussian pulse with parameters $\sigma_\tau = 2$ and $\omega_r = 3$.

As can be seen, the frequency space electric field profile attained using the fast Fourier transform aligns with the analytical profile. This shows that this algorithm is sufficiently robust for use on other arbitrary pulses in which the analytical solution is not defined, such as stochastic FEL pulses.

Autocorrelation of coherent Gaussian pulse Using Eq. (2.53), the nonstationary first order autocorrelation was calculated for a Gaussian coherent pulse. This was compared with the approximation from Eq. (2.56) by plotting the two functions simultaneously, as shown in figure 19. From this nonstationary autocorrelation calculation, the coherence time of the pulse was calculated also.

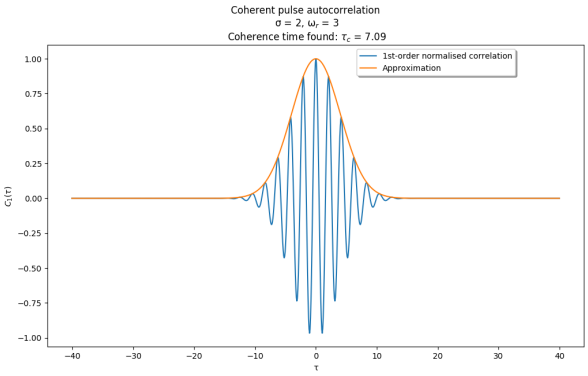

Figure 19: Autocorrelation function plots of a coherent Gaussian pulse

As can be seen from figure 19, the coherent pulse autocorrelation matches exactly with the approximation described by Eq. (2.56). The coherence time was found to satisfy Eq. (2.57), with a value of 7.09, rounded to two decimal places.

4.2.2 Modelling a pulse with uniform arrival time probability density profile

To investigate the shot noise model of a pulse resulting from uniformly random electron bunch density, the stochastic term of Eq. (2.49) was isolated and modelled. Figure 20 shows the electric field and intensity profiles for this stochastic expression for a single radiation pulse (which is itself a superposition of radiation from many contributing electrons) and for the average of 500 pulses.

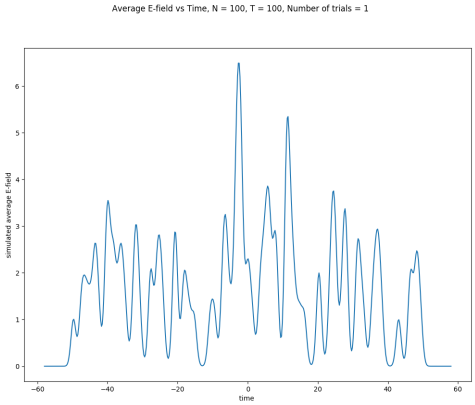

(a) E-field of pulse vs time for single shot

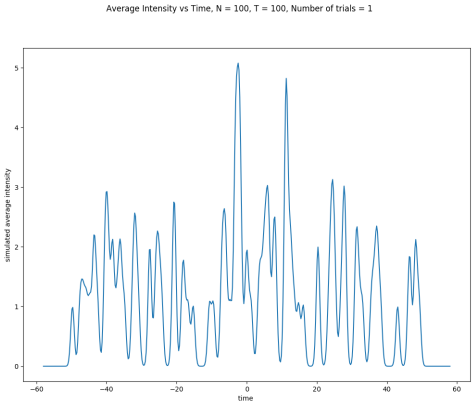

(b) Intensity of pulse vs time over single shot

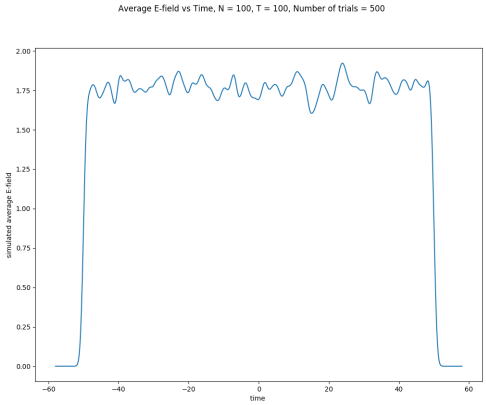

(c) E-field of pulse vs time averaged over 500 trials

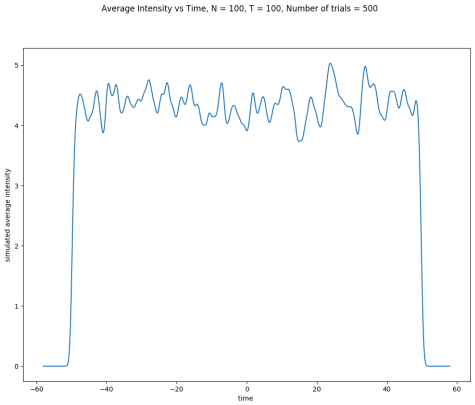

(d) Intensity of pulse vs time averaged over 500 trials

Figure 20: E-field and intensity profiles of pulse resulting from uniform electron bunch density along time domain.

Figures 20(a) and 20(b) show a single shot pulse composed of noisy signals with spikes uniformly distributed over the bunch length T_b. Figures 20(c) and and 20(d) show that over a large number of trials, the signal resembles that of a square pulse, with approximately constant expected values $\langle E(t) \rangle$ and $\langle I(t) \rangle$ for times t within the bunch length.

The parameters used in this simulation are $N_e = T_b = 100$. From Eq. (3.11), the analytically predicted expected value of the electric field for times t within the bunch length interval $\left[-\frac{T}{2}, \frac{T}{2}\right]$ is calculated to be $E\left[E(t)\right] \simeq 1.77$. Figure 20(c) confirms that this expression is correct, since the magnitude of the average electric field has an approximate value of 1.77 within the bunch length interval.

4.2.3 Modelling a pulse with Gaussian arrival time probability density profile

FEL radiation with Gaussian electron bunch statistics were investigated, using Eq. (2.51) but with the stochastic term being isolated. The E-field and intensity profiles of pulse resulting from Gaussian electron bunch density are plotted in the time domain in figure 21. The single-shot pulse electric field

and intensity profiles are seen in (a) and (b), respectively, and the Monte Carlo averaged pulse over 500 trials is shown in (c) and (d), respectively.

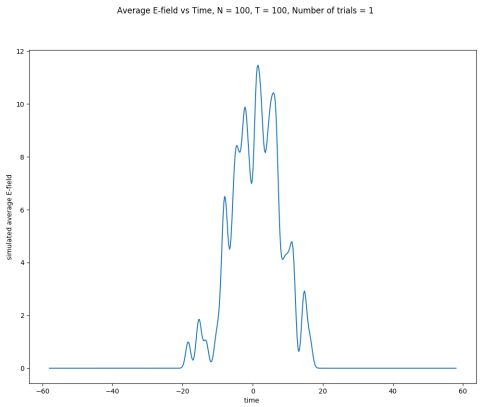

(a) E-field of pulse vs time for a single shot

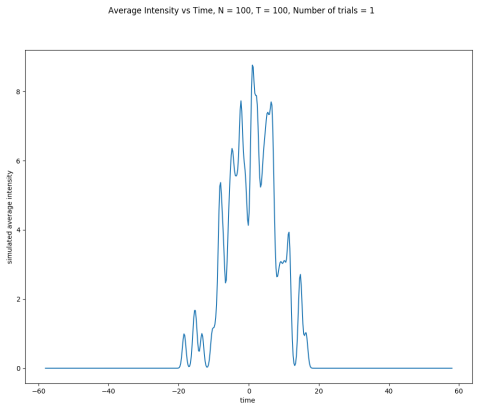

(b) Intensity of pulse vs time for a single shot

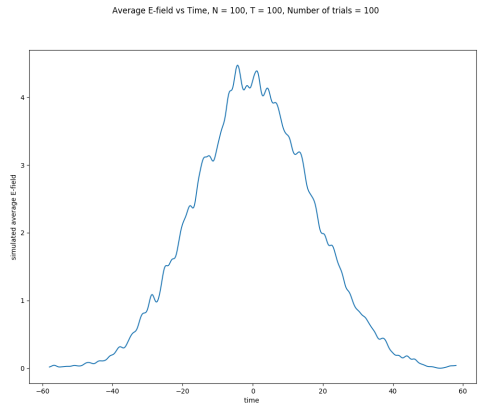

(c) E-field of pulse vs time averaged over 500 trials

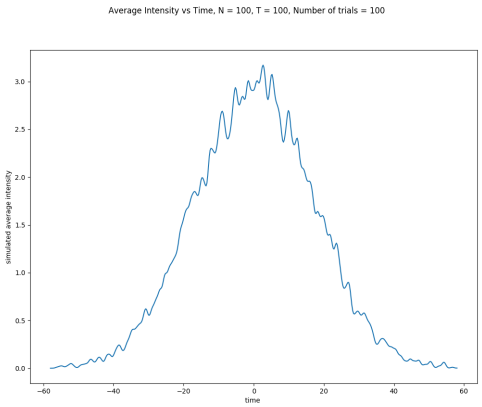

(d) Intensity of pulse vs time averaged over 500 trials

Figure 21: E-field and intensity profiles of pulse resulting from Gaussian electron bunch density along time domain

Figures 21(a) and 21(b) show a single shot pulse. It can be seen that there are spikes in the magnitude of both the electric field and intensity, concentrated predominantly around $t = 0$. Figures 21(c) and and 21(d) show that over a large number of trials, the signal resembles that of normal distribution centred around $t = 0$. Thus, since the other terms of Eq. (2.51) do not vary with time when taken over a large sample of independent pulses (cosine term and constants), the statistics of the radiation pulse in time have been shown to follow a Gaussian distribution centred about $t = 0$.

4.2.4 FEL SASE radiation with uniform electron bunch density profile

The electric field and intensity of FEL pulses with uniform electron bunch density were modelled computationally in the time domain using Python. By simulating this stochastic model many times, a large ensemble of data was attained for the electric field and intensity as a function of time. Using this data,

the autocorrelation and power spectral density of the FEL radiation were also found. An investigation of the average intensity as a function of the number of electrons per bunch was also conducted by taking Monte Carlo trials of intensity and varying the number of electrons per bunch, N_e. The results of these simulations are presented below.

Electric field and intensity profiles in time domain Shown in figure 22 are the plots of this stochastic radiation in the time domain.

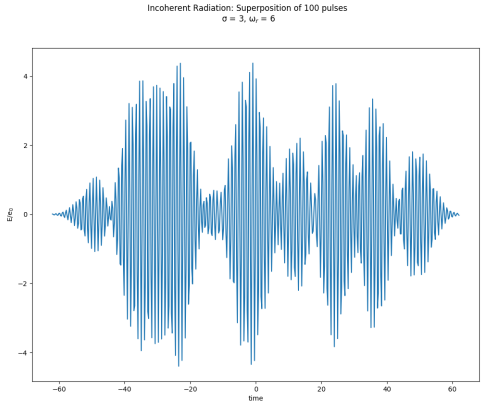

(a) Electric field profile in time domain, single shot

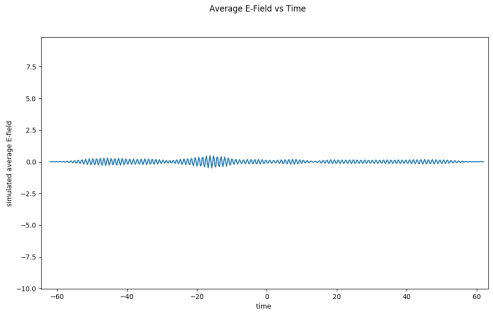

(b) Electric field profile in time domain, 100 trials

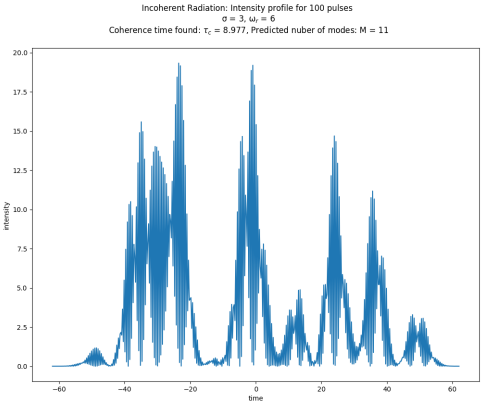

(c) Intensity profile in time domain, single shot

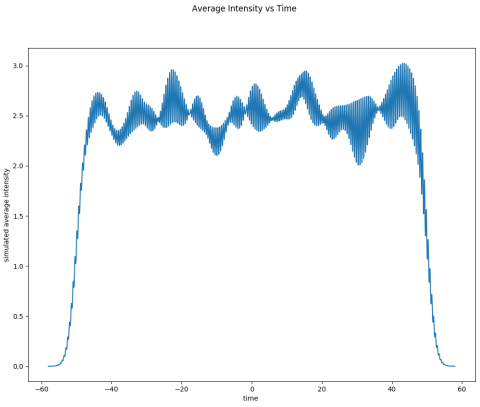

(d) Intensity profile in time domain, 100 trials

Figure 22: Electric field and intensity profiles for FEL SASE radiation with uniform electron bunch density in the undulator

From figure 22 it is seen that, as with the stochastically isolated model in 4.2.2, the electric field and intensity for a single shot fluctuates in time. Taking the average over many trials reveals that the intensity profile resembles a square pulse within the bunch length T_b, indicating that the intensity is time-invariant. The ensemble average of the electric field is seen to go to zero for all t.

Average intensity dependence on number of electrons in bunch Shown in figure 23 is the plot of the average intensity of SASE radiation vs the number of contributing electrons in the bunch.

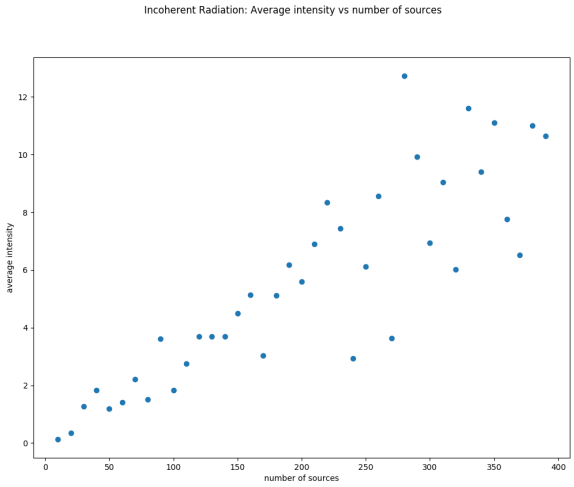

Figure 23: FEL SASE radiation intensity as a function of the number of contributing electron sources in the pulse

As seen from figure 23, the average intensity is directly proportional to the number of electrons in the bunch. This is a reasonable result, since as the number of electrons in the bunch increases, so too does the number of sources of radiation.

Autocorrelation Shown in figure 24 are the plots of the first and second order autocorrelation functions taken at $t = 0$ and $t = 10$.

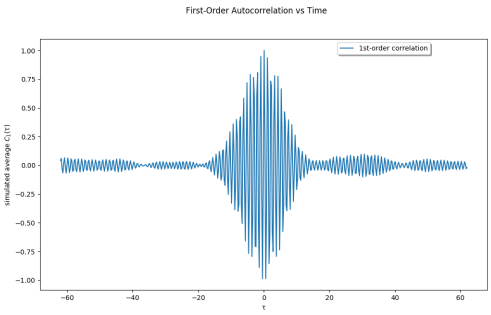

(a) First-order autocorrelation taken for $t = 0$

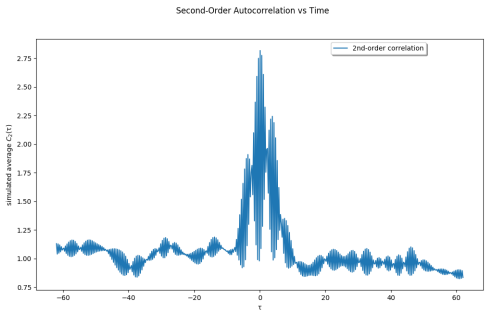

(b) Second-order autocorrelation taken for $t = 0$

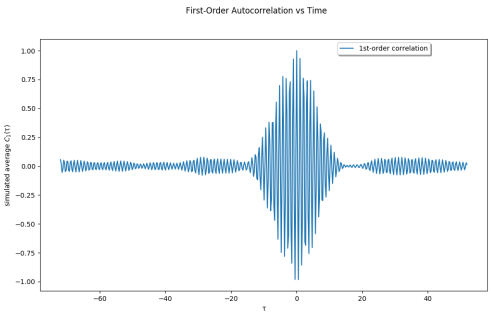

(c) First-order autocorrelation taken for $t = 10$

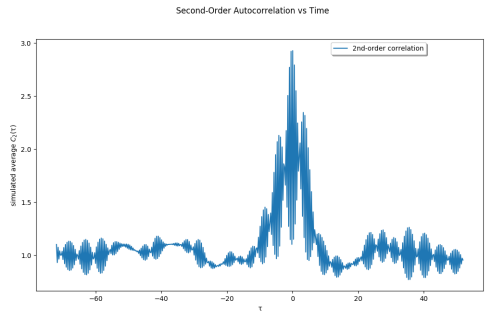

(d) Second-order autocorrelation taken for $t = 10$

Figure 24: Autocorrelation for an FEL pulse with uniform electron bunch density (for 500 Monte Carlo runs)

From figure 24 it is seen that both the first and second order autocorrelation functions taken at $t = 0$ has the same profile in time change τ as the autocorrelation taken at $t = 10$. This implies that the autocorrelation is time invariant. From this, coupled with the average electric field and intensity results above, it is seen that this pulse conforms to the properties of a wide-sense stationary random process.

Power spectral density Shown in figure 25 are the magnitude and phase components of the power spectral density.

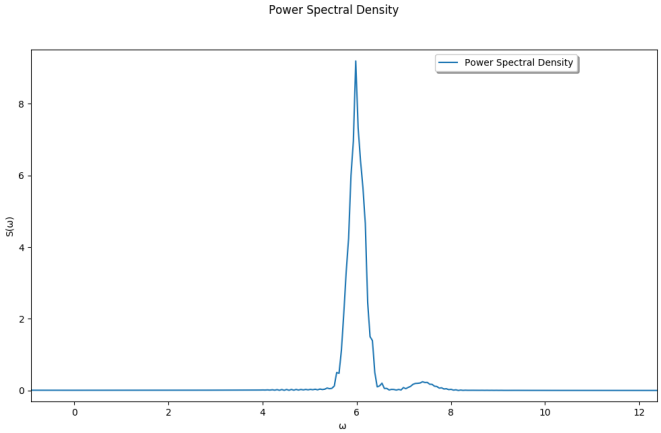

(a) Magnitude spectrum

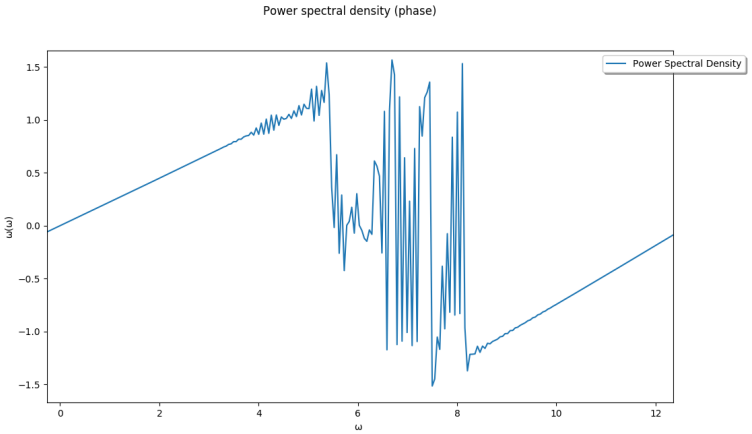

(b) Phase spectrum

Figure 25: Power spectral density for an FEL pulse with uniform electron bunch density (for 500 Monte Carlo runs)

As predicted, there is a peak at the resonance frequency in the magnitude spectrum for the power spectral density. The phase spectra demonstrates large fluctuations in the phase outside of a small band of frequencies around the resonance frequency, where the phase is approximately zero. This indicates that the pulse has coherent in frequency space in this band but incoherent elsewhere.

4.2.5 FEL SASE radiation with Gaussian electron bunch density profile

By analysing the simulated statistical properties of SASE FEL radiation based on a Gaussian electron bunch density profile, a comparison can be made between the behaviour of the Gaussian bunch density pulse and the uniform bunch density pulse.

The electric field and intensity of FEL pulses with Gaussian electron bunch density were modelled computationally in the time domain using Python. By simulating this stochastic model many times, a large ensemble of data was attained for the electric field and intensity as a function of time. Using this data, the autocorrelation and power spectral density of the FEL radiation were also found. The results of these simulations are presented below.

Electric field and intensity profiles of in time domain Shown in figure 26 are the plots of this stochastic radiation in the time domain.

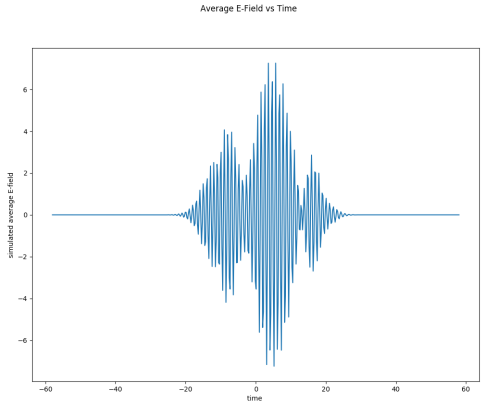

(a) Electric field profile in time domain, single shot

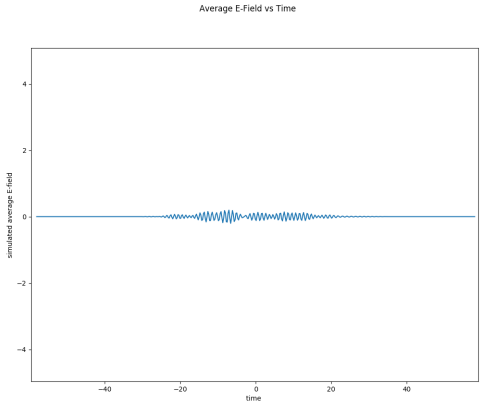

(b) Electric field profile in time domain, 100 trials

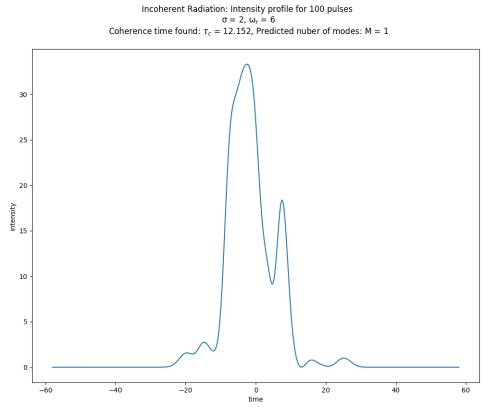

(c) Intensity profile in time domain, single shot

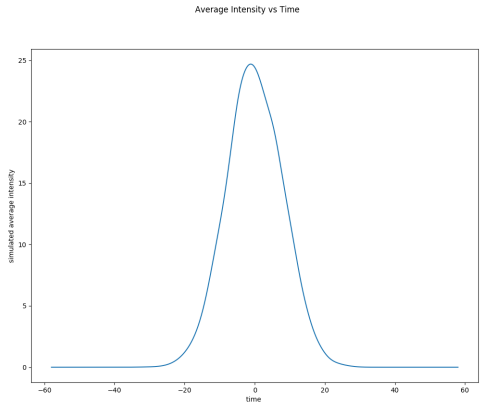

(d) Intensity profile in time domain, 100 trials

Figure 26: Electric field and intensity profiles for FEL SASE radiation with Gaussian electron bunch density in the undulator

The single-shot profile shows spikes in intensity and electric field in time but is concentrated around $t = 0$, unlike in the uniform bunch density case, where spiking occurred at random times. The Monte Carlo trials for this pulse profile reveal that the averaged electric field goes to zero, while the average intensity is shown to be a Gaussian distribution centred on $t = 0$.

Autocorrelation Shown in figure 27 are the plots of the first and second order autocorrelation functions taken at $t = 0$ and $t = 10$.

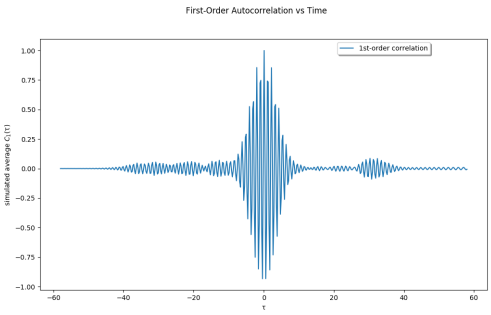

(a) First-order autocorrelation taken for $t = 0$

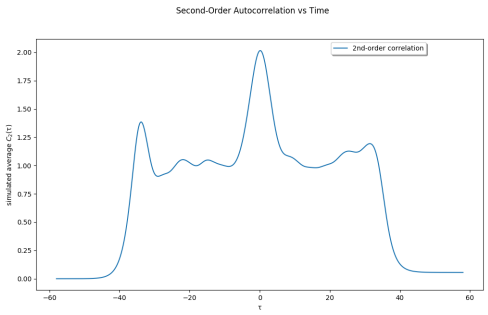

(b) Second-order autocorrelation taken for $t = 0$

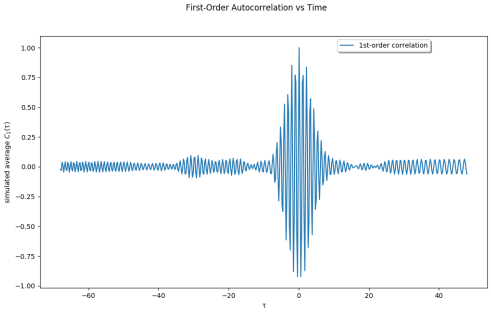

(c) First-order autocorrelation taken for $t = 10$

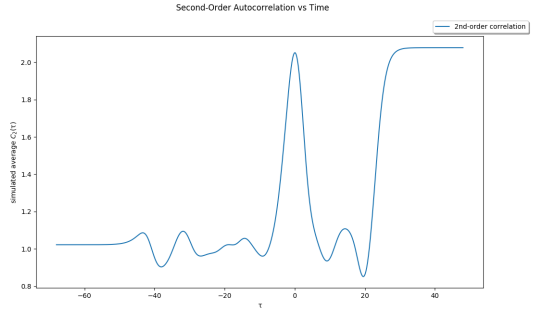

(d) Second-order autocorrelation taken for $t = 10$

Figure 27: Autocorrelation for an FEL pulse with Gaussian electron bunch density (for 500 Monte Carlo runs)

From figure 27 it is seen that the first and second order autocorrelation functions are not time invariant in the case of Gaussian electron bunch density, since, despite having similar peaks at $\tau = 0$, the magnitude of the autocorrelation does not match in time with its corresponding time-shifted counterpart, for cases of both first and second order autocorrelation functions. This verifies that this is not a stationary process.

Power spectral density Shown in figure 28 are the magnitude and phase components of the power spectral density. It should be noted that the autocorrelation function used in the calculation of the power spectral density was different from that plotted in figure 27 above. In modelling the power spectral density for the case of a Gaussian electron bunch density, nonstationary process statistics were assumed and hence the time-average autocorrelation was used, seen in Eq. (2.53).

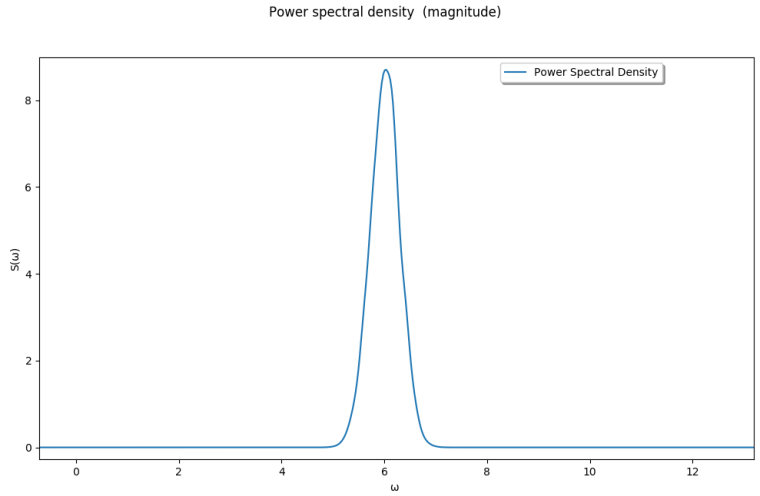

(a) Magnitude spectrum

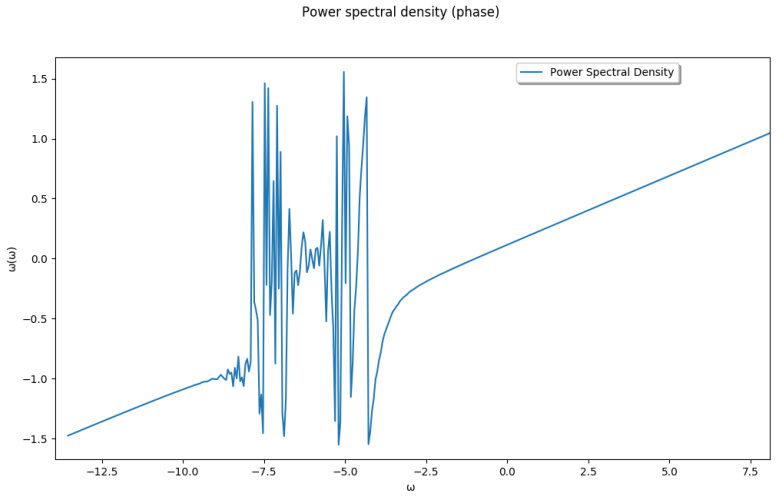

(b) Phase spectrum

Figure 28: Power spectral density for an FEL pulse with Gaussian electron bunch density (for 500 Monte Carlo runs)

From figure 28, it is seen that the PSD magnitude spectrum contains a peak centred about the pulse's resonance frequency, $\omega_r = 6$. The phase spectrum reveals large levels of fluctuation outside the resonance frequency, while having approximately zero phase in a narrow band at $-\omega_r$. It's worth noting that the phase spectrum of the power spectral density shows the point of zero phase in the frequency space to be negative. This is likely due to the smoothing term, $\chi = 1 + \frac{i}{\sqrt{3}}$,introduced in Eq. (2.51).

5 Conclusion

In this project the statistical properties of various forms of Brownian motion were obtained by conducting Monte Carlo trial simulations with sufficiently large sample size. The simulated results presented in this project reflect the behaviour of real-world physical systems that share the same statistical properties, as in the Ornstein-Uhlenbeck model.

It was shown that FEL SASE radiation resulting from uniformly random shot noise has a uniformly random intensity profile in the time domain for the duration of the pulse. For FEL radiation produced in the uniform electron bunch density regime, the electric field profile was shown to have the statistical properties of a wide-sense stationary stochastic process. The Gaussian electron bunch density pulse has an electric field profile that was shown to be determined in terms of a stationary Gaussian random process, as seen from the ensemble average intensity profile in figure 26(d). In addition, many other statistical properties of FEL SASE radiation were investigated and presented in this project.

Due to time constraints, there are some areas of analysis that haven't been covered in this project, such as a verification of the analytical expressions provided for the coherence time and number of modes by Krinsky and Li (2006), or simulations conducted to model the range of spectral coherence Ω_{coh} for a stochastic FEL pulse. Doing so would provide a more comprehensive analysis of the temporal behaviour of FEL SASE radiation based on the model of shot noise.

6 Appendix

6.1 Source code used in this project

All source code used in this project can be found at https://github.com/aaronlf/Brownian-motion-project.

6.2 Derivation of the expectation value of an isolated FEL pulse with uniform electron bunch density

Let $g(x)$ be a real-value function of the real line, $g : \mathbb{R} \to \mathbb{R}$.

Let X be a random variable and let

$$Y = g(X) \tag{6.1}$$

Then Y is also a random variable.

The distribution of Y can be derived from the distribution of X. If the equation $g(x) = y$ has n solutions $\{x_1, ..., x_n\}$, then

$$f_Y(y) = \sum_{k=1}^{n} f_X(x) \left| \frac{dx}{dy} \right|_{x=x_k} = \sum_{k=1}^{n} \frac{f_{X(x_k)}}{|g'(x_k)|} \tag{6.2}$$

where $g'(x_k)$ is the derivative of $g(x)$ evaluated at x_k.

The expectation value of a random variable Y can be found if the probability distribution $f_Y(y)$ is known:

$$\mathbb{E}[Y] = \int_a^b y f_Y(y) dy, \quad for\ a < y < b \tag{6.3}$$

Isolating only the stochastic contribution of the pulse, let the electric field be given by,

$$E(t) = \sum_{j=1}^{N_e} E_0(t, t_j) = \sum_{j=1}^{N_e} e^{-(t-t_j)^2} \tag{6.4}$$

For a single electron, let $X = t - t_j$. Thus one can say,

$$\begin{aligned} X &= t - U\left[-\frac{T}{2}, \frac{T}{2}\right] \\ &= t - U\left[t - \frac{T}{2}, t + \frac{T}{2}\right] \end{aligned} \tag{6.5}$$

It can be be noted that for a uniformly distributed random variable, the probability density function (PDF) describing it is given by,

$$f_U(x) = \begin{cases} \frac{1}{b-a}, & a < x < b \\ 0, & \text{elsewhere} \end{cases} \tag{6.6}$$

and hence for X as defined above one arrives at the following distribution function:

$$f_X(x) = \begin{cases} \frac{1}{T}, & t - \frac{T}{2} < x < t + \frac{T}{2} \\ 0, & \text{elsewhere} \end{cases} \tag{6.7}$$

What's important to note is that $f_X(x)$ is not at all dependent on the value of t, so long as $t - \frac{T}{2} < x < t + \frac{T}{2}$ is satisfied.

Now, let $Y = e^{-X^2}$. This represents one single electron contribution to the pulse, with $X = t - t_j$ as defined above.

The equation $y = e^{-x^2}$ has the following solutions (for $0 < y \leq 1$):

$$x_1 = \sqrt{-ln(y)}, \qquad x_2 = -\sqrt{-ln(y)} \tag{6.8}$$

Finding the derivative of y with respect to x gives:

$$\left.\frac{dy}{dx}\right|_{x=x_1} = \left.\frac{dy}{dx}\right|_{x=x_2} = 2y\sqrt{-ln(y)} \tag{6.9}$$

Thus, the PDF of y is given by,

$$f_Y(y) = \sum_{k=1}^{n} \frac{f_X(x_k)}{|g'(x_k)|} = \frac{1}{Ty\sqrt{-ln(y)}} \tag{6.10}$$

The expectation value of Y is given by,

$$\begin{aligned} \mathbb{E}[Y] &= \int_0^1 y f_Y(y) dy = \frac{1}{T} \int_0^1 \frac{1}{\sqrt{-ln(y)}} dy \\ &= \frac{\sqrt{\pi}}{T} \end{aligned} \tag{6.11}$$

Note that $X = t - t_j$ is identically and independently distributed for $t - \frac{T}{2} < x < t + \frac{T}{2}$. This means that Y is identically and independently distributed when $t - \frac{T}{2} < x < t + \frac{T}{2}$.

Now, let's apply this theory to a scenario with N_e independent electron contributions. The expected value of $E(t)$ is given by:

$$\langle E(t) \rangle = \mathbb{E}\left[Y_1 + Y_2 + ... + Y_{N_e}\right] = \mathbb{E}\left[Y_1\right] + \mathbb{E}\left[Y_2\right] + ... + \mathbb{E}\left[Y_{N_e}\right] \tag{6.12}$$

since Y_i is independently and identically distributed.

One can write,

$$\langle E(t) \rangle = \frac{N_e \mathbb{E}\left[Y_1\right]}{T} \tag{6.13}$$

References

[1] Brown, R. A brief account of microscopical observations on the particles contained in the pollen of plants and the general existence of active molecules in organic and inorganic bodies. Edinburgh New Philosophical Journal:1828;358–371. Available from: `https://en.wikisource.org/wiki/The_miscellaneous_botanical_works_of_Robert_Brown/Volume_1/A_brief_account_of_microscopical_observations_made_on_the_particles_contained_in_the_pollen_of_plants`

[2] Black F, Scholes M. The Pricing of Options and Corporate Liabilities. J Polit Econ. 1981;(3):637–54.

[3] Brady S. Construction and Properties of Brownian Motion [Internet]. Department of Mathematics, University of Hawai'i at Mānoa. 2006. Available from: `http://math.hawaii.edu/home/talks/brady_talk.pdf`

[4] Bachelier, L. (1900). Théorie de la Spéculation, Annales Scientifique de l'École Normale Supérieure, 3e série, tome 17, 21-86.

[5] Einstein, A. Über die von der molekularkinetischen Theorie der Wärme geforderte Bewegung von in ruhenden Flüssigkeiten suspendierten Teilchen (Investigations on the theory of Brownian movement). Annalen der Physik. 1905;17:549–560.

[6] von Smoluchowski. M. Zur kinetischen Theorie der Brownschen Molekularbewegung und der Suspensionen. Annalen der Physik. 1906;21:756– 780.

[7] Dardo M. Nobel Laureates and Twentieth-Century Physics. Cambridge University Press; 2004. 114-116 p.

[8] Wiener N. The average of an analytical functional and the Brownian movement. Proc Nat Acad Sci USA. 1921;(7):294–8.

[9] Uhlenbeck GE, Ornstein LS. On the theory of Brownian motion. Phys Rev. 1930;36(5):823–41.

[10] Johnson J. Thermal Agitation of Electricity in Conductors. Phys Rev. 1928;32(97):97–109.

[11] Nyquist H. Thermal Agitation of Electric Charge in Conductors Phys. Rev. Phys Rev. 1928;32(110):110–113.

[12] Stokes GG. On the effect of internal friction of fluids on the motion of pendulums Transactions of the Cambridge Philosophical Society. Trans Cambridge Philos Soc. 1851;(9):part ii: 8–106.

[13] Wiener N. Generalized Harmonic Analysis. Acta Math. 1930;55:117–258.

[14] Khintchine A. Korrelationstheorie der stationären stochastischen Prozesse. Math Ann. 1934;109(1):604–14.

[15] Schottky W. Über spontane Stromschwankungen in verschiedenen Elektrizitätsleitern. Ann Phys. 1918;57:541–67.

[16] Rice SO. Mathematical analysis of random noise. Bell Syst Tech J. 1945;24:46–156.

[17] Berrah N, Bozek J, Costello JT, Düsterer S, Fang L, Feldhaus J, et al. Non-linear processes in the interaction of atoms and molecules with intense EUV and X-ray fields from SASE free electron lasers (FELs). J Mod Opt. 2010;57(12):1015–40.

[18] Middleton DPW, Nikolopoulos LAA. Effects of autoionising states on the single and double ionisation yields of neon with soft X-ray fields. J Mod Opt. 2012;59(19):1650–63.

[19] Li Y, Krinsky S. Statistical analysis of the chaotic optical field from a self-amplified spontaneous-emission free-electron laser. Phys Rev. 2006;73(6).

[20] Goodman JW. Statistical optics. 1st ed. John Wiley & Sons, New York; 1985.